2. The Group of Cs_2MX_4-type Crystals with Incommensurate (IC) Phases: Cs_2CdBr_4, Cs_2HgBr_4, Cs_2CdI_4 and Cs_2HgCl_4 -Dynamic Properties at Normal-Incommensurate Phase Transitions and in IC Phases -

2.1 Introduction

Translational lattice periodicity is one of the basic characteristics in a crystals (Fig. 1. 1 (a)). It is known, however, that a group of crystals can not be described by a single translational period but require two or more sublattices which have incommensurate lattice lengths for each other (Fig. 1. 1 (b)) [1, 2]. These crystals are so-called incommensurate (IC) crystals. Some substances form a incommensurate crystal in a specific temperature range [1]. They usually form a normal crystal lattice in a high temperature phase, while the incommensurately modulated sublattice locks in a commensurate length in a low temperature phase (Fig. 1. 1.(c)) [2]. It has been observed in the most cases that the normal to incommensurate phase transition is of 2nd order and the incommensurate to commensurate phase transition is 1st order [1].

Many compounds of the A_2BX_4 family with the pseudo-hexagonal β-K_2SO_4 type structure (*Pnma*) as shown in Fig. 2. 1 have phase transitions and exhibit an IC phase at low temperatures. Most of them, *e.g.*, K_2SeO_4 and Rb_2ZnCl_4, etc., form the IC phase described by an IC modulation vector, $q_{IC} = (1-\delta)a^*/3$, parallel to the pseudo-hexagonal axis with a parameter δ which increases with temperature decrease. Phase transitions from the IC phase to a commensurate (C) phase at a low temperature given by T_C occur at the wave vector $q_C = a^*/3$, and a 3-fold superstructure belonging to $Pna2_1$ appears [1].

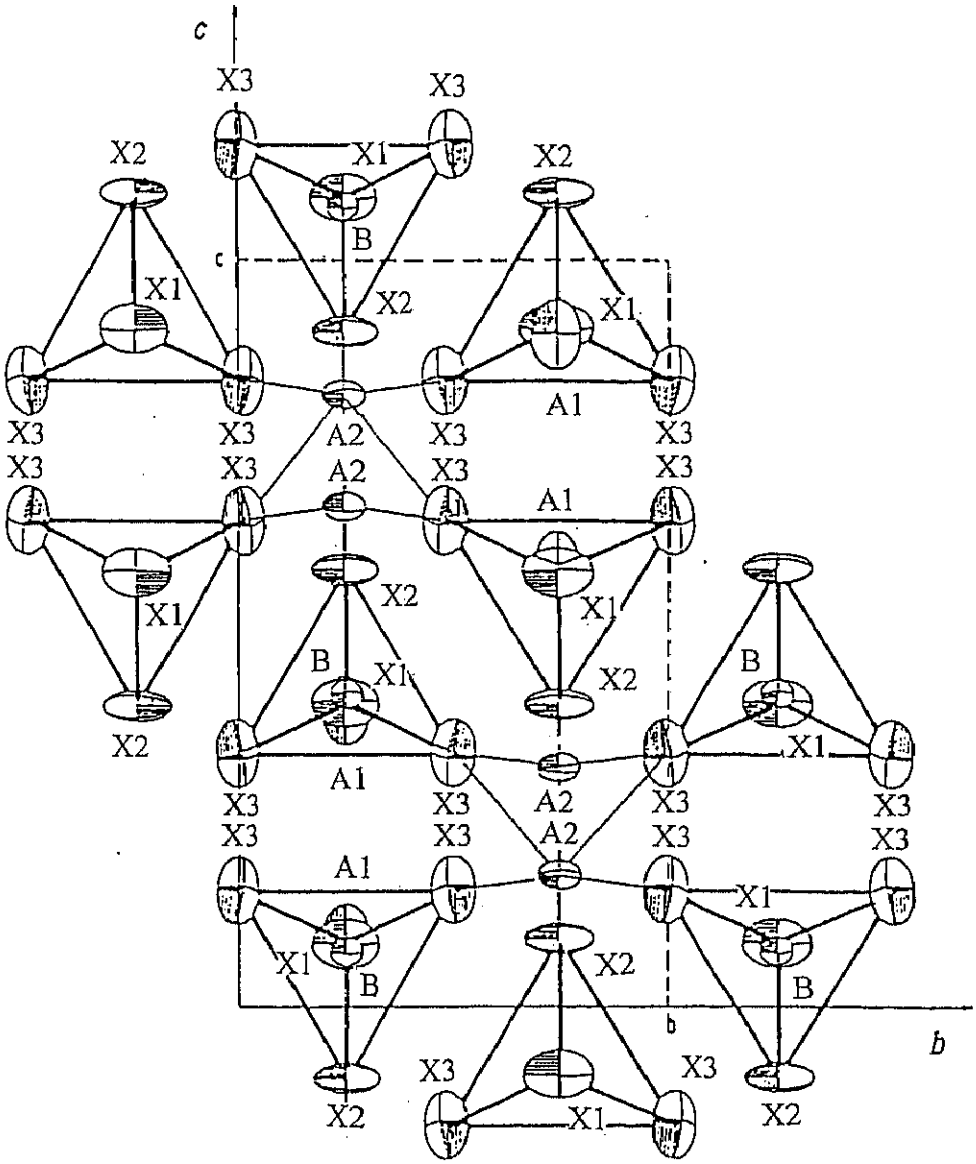

Fig. 2. 1 Crystal Structure in A_2BX_4 compounds with the β-K_2SO_4-type structure (*Pnma*, $Z = 4$) in *bc*-plane. Two crystallographically nonequivalent A sites, A1 and A2, are in this structure.

In this chapter, the dynamic behavior of the crystal lattice in the group of Cs_2MX_4 (Cs_2CdBr_4, Cs_2HgBr_4, Cs_2CdI_4 and Cs_2HgCl_4) crystals with incommensurate phases are discussed by use of the results of ^{133}Cs NMR T_1 measurements in respective phases. Especially, the dynamics in the IC phase and critical behavior near the N-IC phase transiton are compared with each other in measured substances and the bond properties between halogen and Cs atoms in crystals are discussed in detail.

2.2 Theory

2.2.1 NMR spin-lattice relaxation time T_1

In the present system, the main mechanism of ^{133}Cs NMR relaxation is the fluctuation of the quadrupole interaction caused by motions of ions or molecules contained in crystals, where only lattice vibrations are enough to be considered as the relaxation mechanism, because the contribution from molecular motions such as the rotation of complex anions can be neglected in the low-temperature region below 400 K in ionic crystals as studied in this work.

The lattice modes can be classified into three categories: The first is the normal lattice modes which contribute to the relaxation in all temperature range [3]. The second is the critical fluctuation which comes to the front near the 2nd order phase transition temperature [4]. The 3rd is IC fluctuations which are characteristic in the IC phase [2]. The net spin-lattice relaxation rate can be represented as the sum of these contributions. The formalizations of contributions to the NMR relaxation from these lattice modes are described as follows.

• *Contribution from Normal Lattice Vibrations*

At first, the contribution from normal lattice vibrations is discussed. The spin lattice relaxation from this origin is induced by the spin-phonon coupling which is represented by a Hamiltonian:

$$\hat{H} = FA,$$

where F and A are the lattice and the spin operator, respectively. F can be expanded by powers of lattice distortion W,

$$F = F_1 W + F_2 W^2 + F_3 W^3 + \cdots. \tag{2.1}$$

Quantum mechanically, the i-th term F_i causes a process of i phonons absorption or emission. Since W is small, the eq. (2.1) converges although F_is are all the same order of magnitude [3].

Since the frequencies of the lattice vibrations are much higher than the NMR Larmor frequency $\nu_L=\omega_L/2\pi$, the two-phonon Raman process, in which one phonon of an angular frequency ω is absorbed and another one of angular frequency ω' is emitted, is much more effective than the one-phonon direct process or the other two-phonon processes in which both of two phonons are simultaneously absorbed or emitted. This is because all phonons in the Raman process fulfilling the relation $\omega - \omega' = \pm \omega_L$ take part in the NMR relaxation. The quadrupolar relaxation rate T_{1l}^{-1} contributed from the thermal lattice vibration via the two-phonon Raman process is represented by the

relation using the two phonon operator F_2 given by [3]

$$T_1^{-1} \propto \frac{81\pi}{2}\left(\frac{F_2\hbar}{mv^2}\right)^2 \int_0^{\Omega} \frac{e^{\hbar\omega/kT}}{(e^{\hbar\omega/kT}-1)^2}\frac{\omega^6}{\Omega}d\omega, \tag{2.2}$$

where m, v and Ω are the mass and velocity of a vibrating atom and the cutoff frequency, respectively. The magnitude of spin-phonon coupling concerning F in ^{133}Cs NMR is determined by the amplitude of quadrupole coupling fluctuation $\Delta e^2Qq/h$ caused by lattice vibrations. Since lattice vibrations in Cs_2MX_4 crystals fluctuate interactions between Cs^+ cations and MX_4^{2-} anions, weak covalency formed between the cations and anions is expected to be modulated by the vibrations. Then F_2 can be related with the electric field gradient vibration mode by this covalency. This effect can be given by[3]

$$F_2 \propto \Delta e^2 Qq/h \propto \lambda'\left\langle\frac{1}{r^3}\right\rangle, \tag{2.3}$$

where λ' is the degree of covalency between Cs^+ and MX_4^{2-} and r is the distance between the nucleus and the electron related to that bond. The dependence of λ' on inteionic distance R with the unit of Å, has been assumed as [5]

$$\lambda' \propto \exp(-R/0.345), \tag{2.4}$$

which is related with the Born-Mayer interionic repulsion potential [6].

In the high-temperature limit, i.e., $kT >> \hbar\Omega = k\theta_D$ where θ_D is the Debye

temperature, eq. (2.1) is rewritten approximately as [3]

$$T_1^{-1} \propto \frac{81\pi}{10}\left(\frac{kT}{mv^2}\right)^2 \frac{F_2^2}{\Omega}. \tag{2.5}$$

Using a temperature independent constant A, eq. (2.5) is rewritten as

$$T_1^{-1} = AT^2 . \tag{2.6}$$

Equations (2.5)-(2.6) can usually be applied as a good approximation even in $T \approx \theta_D$ [3]. On the other hand, in the low-temperature limit $T \langle\langle \theta_D$, eq. (2.1) is represented as

$$T_1^{-1} \propto \frac{81\pi}{2}\left(\frac{F_2\hbar}{mv^2}\right)^2\left(\frac{T}{\theta_D}\right)^7 \Omega. \tag{2.7}$$

・ *Relaxation Caused by Critical Fluctuation*

Near the 2nd order N-IC phase transiton in the N phase, it is expected that the critical fluctuation becomes a dominant mechanism of relaxation. In the IC phase, an anologous mechanism is dominant near the phase transition temperature, though the relaxation behavior in this phase will be discussed later as IC lattice modes. The contribution on the relaxation rate from this mode T_{1c}^{-1} can be derived from the fluctuation-dispersion theorem [7, 8]:

$$T_{1c}^{-1} \propto T \sum_{k} \mathrm{Im}\{\chi(k,\omega_{L})\} / \omega_{L} = T \sum_{k} \chi''(k,\omega_{L}) / \omega_{L}\,, \tag{2.8}$$

where $\omega_L = 2\pi\nu_L$, ν_L is the Larmor frequency and the generalized susceptibility χ (k, ω) is expressed as $\chi'(k, \omega) + i\chi''(k, \omega)$, in which the imaginary part χ'' represents the fluctuation of lattice. The reduced wave vector k is given by the wave vector difference from the incommensurate wave vector q_{IC} as $k = q - q_{IC}$.

Since N-IC transitions in Cs_2MX_4 were considered to be induced by the order-disorder type relaxator mode, the frequency distribution of a monodispersive relaxator fluctuation can be written as [8]

$$\chi(k,\omega) = \chi(k,0)/[1 - i\omega_{L}\tau(k)] \tag{2.9}$$

and

$$\chi(k,0) = \chi(0,0)/[1 + (k\xi)^{2-\eta}]\,, \tag{2.10}$$

where $\tau(k)$ is the relaxation time of lattice, ξ is the correlation length, and η is the critical exponent which characterizes the long-range behavior of the correlation function of susceptibility χ. Replacing the sum in eq. (2.8) by an integral, it is rewritten as[8, 9]

$$T_{1c}^{-1} \propto \frac{\chi(0,0)\,\tau(0)}{\xi^{d}} \int_{0}^{\Lambda\xi} \frac{x^{d-1}dx}{(1 + x^{2-\eta})^{2}}\,, \tag{2.11}$$

where d is the dimensionality of relevant interactions, $k\xi$ is replaced by x, and Λ is a

constant cutoff wave number in the Brillouin zone. Since ξ diverges as $(T-T_{IC})^{-\nu}$ at T_{IC}, the integral can be represented by a constant in the neighborhood of T_{IC}. χ (0, 0) also diverges as $(T-T_{IC})^{\gamma}$ using a critical exponent γ for the susceptibility. Using a reduced temperature $\varepsilon = (T-T_{IC})/T_{IC}$ and a critical exponent $\zeta = \gamma - \nu(d - z)$, a relation:

$$T_{1c}^{-1} \propto \varepsilon^{-\zeta} \tag{2.12}$$

is derived from eq. (2.11), in which z is the dynamical critical exponent [4]. ζ can be obtained from the slope of log T_1 vs. log ε plots in the vicinity of the transition point, because the critical fluctuation is expected to be a dominant mechanism in this temperature region.

The critical exponents depend on the type of interaction which induce the phase transition. From the knowledge of the value of critical exponents, therefore, we can clarify the type of interaction. The nature of interactions driving phase transitions has been formalized for several limiting cases: The first is the mean field approximation under which all crystallographically equal particles feel the same mean field and the Hamiltonian of the system is represented by the Landau equation given by

$$\hat{H} = A(T)\Phi^2 + \cdots,$$

where Φ is the order parameter in this system [10].

The second group of the interaction considers only the first closest interaction and is represented by a quantum mechanical Hamiltonian

$$\hat{H} = \sum_{k}^{n} J_k \cdot S_{1k} S_{2k} \,.$$

This was first introduced for a spin-system and then extended to general phase transitions, where $S = \sum_{k} S$ is a spin or a corresponding state of a particle, J is the strength of the interaction and k represents component of S. In the present system, S is a rotational angle of a complex anion. When the number of components n takes 1,2 and 3, the formula of the interaction are called Ising, XY and Heisenberg, respectively [11, 12]. The values of critical exponent ζ in each model are listed in Table 2. 1 [8, 9, 12, 13].

Table 2.1 *Critical exponent ζ for the order-disorder type relaxator mode in the each model of the interaction.*

Dimension d	Model	critical exponent ζ	Dimension d	Model	critical exponent ζ
–	mean field	1/2	3	XY	0.625
2	Ising	3/2		Heisenberg	0.659
3	Ising	0.592	3	spherical	1

・ *Relaxation Caused by Incommensurate Fluctuation*

The NMR T_1 in the IC phase is often short compared with those in N and C phases [1, 2]. This anomalous NMR relaxation can be attributed to IC fluctuations. In the IC phase, the displacements of atoms (denoted by open circle in Fig. 1. 1(b)) from positions in the N phase are represented by the incommensurate modulation wave. This modulation wave is generally oscillates and expressed by two components with fluctuations of amplitude and phase of the wave so called the amplitudon and the phason, respectively (Fig. 2. 2) [2, 14].

This IC modulation wave can ideally be described by a plane wave, however in real system, atoms are biased to one-side especially in the low temperature region (Fig. 2. 3) [15, 16] and consists of small commensurate domains. Domain walls, where the phase of the modulation wave quickly changes, are called as phase solitons. When the incommensurate phase can be described by this soliton model, it is called the multi-soliton limit. Then the phason branch splits to acoustic and optical parts which correspond to phase oscillations in the commensurate domains and domain walls, respectively (Fig. 2. 3) [2].

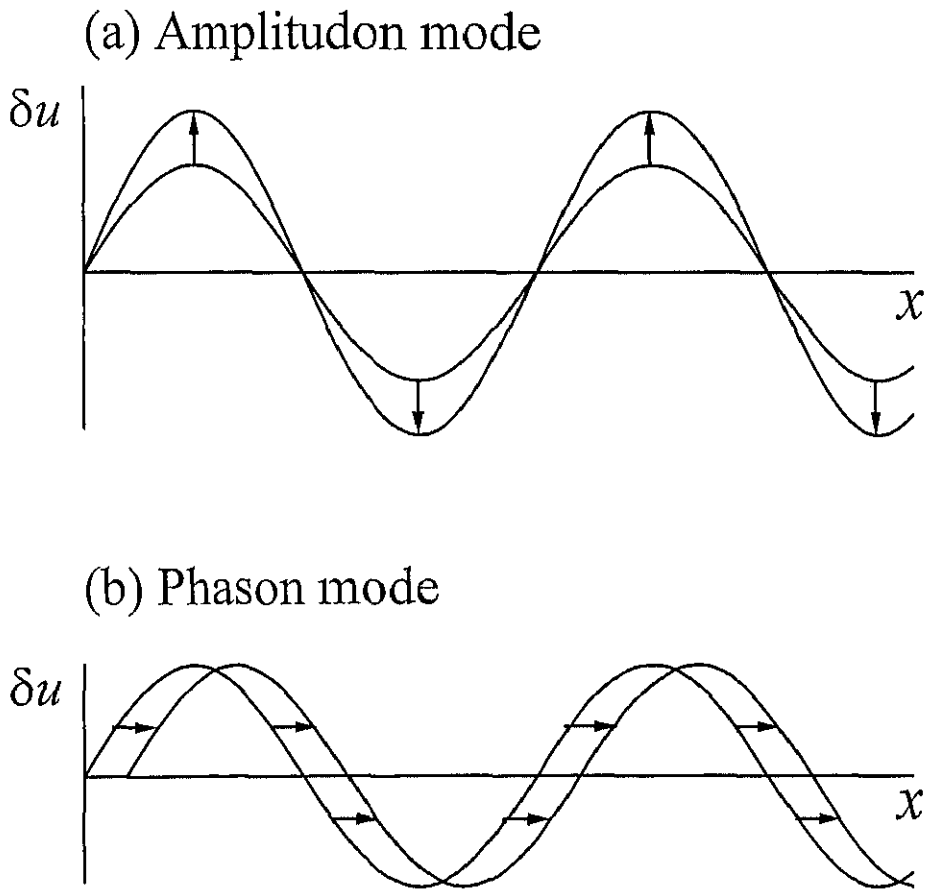

Fig. 2. 2 (a) Amplitudon and (b) phason modes which are fluctuations in amplitude and phase, respectively, in the plane wavelike incommensurate modulation wave.

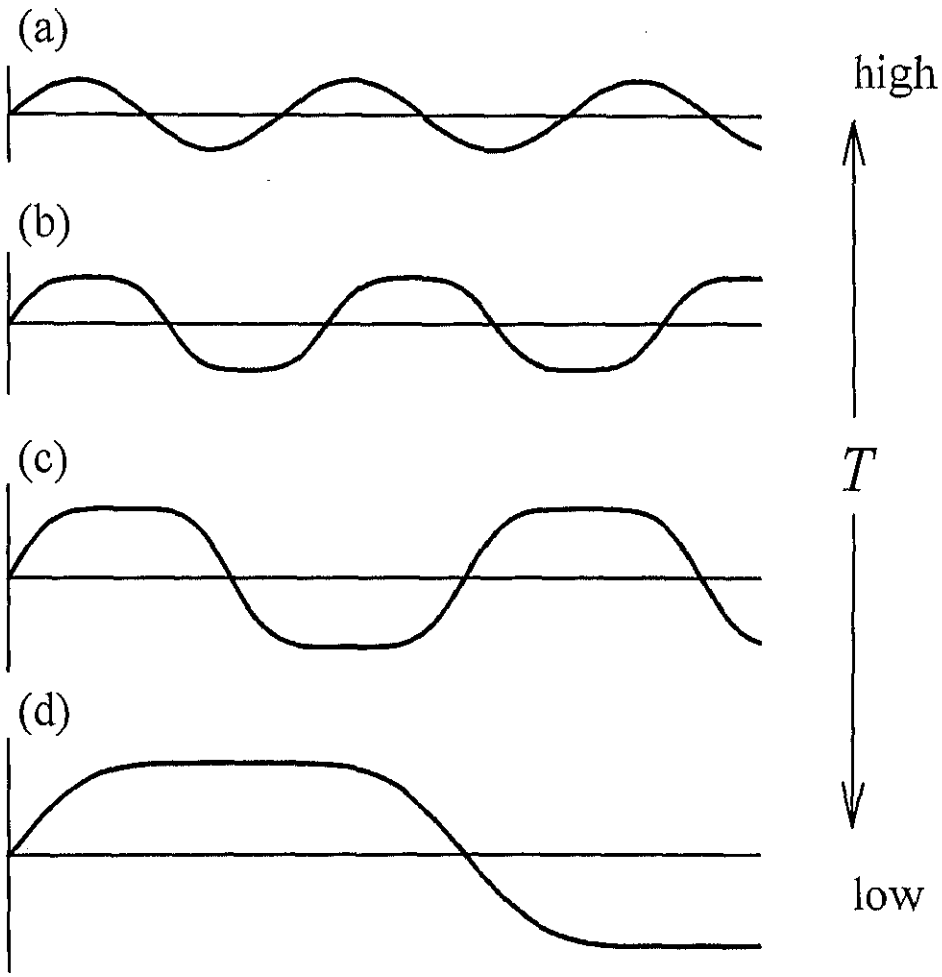

Fig. 2. 3 Temperature dependences of the incommensurate modulation wave. The modulation is represented by the continuous sinusoidal plane wave just below the N-IC phase transition temperature (a) and getting more multi-soliton type with decreasing temperature (b)-(d). In the multi-soliton limit, the modulation wave consists of commensurate domains, where the phase of the modulation wave is constant, and domain walls where the phase changes abruptly.

The relaxation rate T_1^{-1} in the IC phase can be represented by the sum of contributions from the amplitudon and the phason given by T_{1a}^{-1} and $T_{1\phi}^{-1}$, respectively, in addition to the usual lattice vibration as

$$T_1^{-1} = T_{1l}^{-1} + T_{1a}^{-1} + T_{1\phi}^{-1}. \tag{2.13}$$

Here, the amplitudon behaves analogous to the critical mode and T_{1a}^{-1} is given by [2]

$$T_{1a}^{-1} \propto (T_{IC} - T)^{-\zeta'}, \tag{2.14}$$

where ζ' is the critical exponent of T_{1a}^{-1} in the low-temperature side of T_{IC}. In most cases, T_{1a}^{-1} shows no frequency dependene except for the very close proximity to T_{IC} because the amplitudon frequency is much higher than the Lamor frequency ω_L [2]. On the other hand, the phason contribution on the relaxation is different in the two limiting cases, the plane wave and the multi-soliton limit [2].

1) Plane Wave Limit

the phason frequency in the plane wave limit is expected to be inappreciably temperature dependent. According to Misho *et al.* [17], the contribution from the relaxatory phason in this limit is represented as

$$T_{1\phi}^{-2} \propto T^2\left(\sqrt{1+\left(\omega_L/\omega_\phi\right)^2}+1\right)^{-1}, \tag{2.15}$$

where ω_ϕ is the phason frequency. In the frequency region of $\omega_\phi \langle\langle \omega_L$, this equation becomes

$$T_{1\phi}^{-1} \propto 1/\sqrt{\omega_L}, \tag{2.16}$$

while in the region $\omega_\phi \rangle\rangle \omega_L$, $T_{1\phi}^{-1}$ is frequency independent. In the other case of displasive type damping oscillation mode, $T_{1\phi}^{-1}$ in the frequency regions of $\omega_\phi \leq \omega_L$ and $\omega_\phi \rangle\rangle \omega_L$ is represented as [2]

$$T_{1\phi}^{-1} \propto \frac{\pi}{2\sqrt{2}} \kappa^{-3/2} \sqrt{\frac{\Gamma}{\omega_L}} \tag{2.17}$$

and

$$T_{1\phi}^{-1} \propto \frac{\pi}{4} \kappa^{-3/2} \frac{\Gamma}{\omega_\phi}, \tag{2.18}$$

respectively, where κ is the constant in the dispersion relation $\omega^2 = \omega_\phi^2 + \kappa k^2$ and Γ the damping constant. Thus, $T_{1\phi}^{-1}$ for the damping oscillation mode is also proportional to $1/\sqrt{\omega_L}$ in the region $\omega_\phi \leq \omega_L$ and independent of ω_L in $\omega_\phi \rangle\rangle \omega_L$.

2) Multi-Soliton Limit

In this limit, the IC phase is understood by the ensemble of commensurate domains separated by fluctuating domain walls so-called phase solitons where the phase changes steeply. Then the phason branch splits to acoustic and optical parts which correspond to phase oscillations in the commensurate domains and fluctuation of domain walls, respectively [2]. Thus $T_{1\phi}^{-1}$ is represented as

$$T_{1\phi}^{-1} = (T_{1\phi})_{ac}^{-1} + (T_{1\phi})_{op}^{-1}, \tag{2.19}$$

where $(T_{1\phi})_{ac}^{-1}$ and $(T_{1\phi})_{op}^{-1}$ are the contribution from acoustic and optical phasons, respectively. Both contributions are lead from the dispersion relations of phasons assuming to be the damping oscillation. The dispersion relation for acoustic phason is represented by [2]

$$\omega^2 = \omega_\phi^2 + \kappa k_\perp^2 + \kappa_z k_z^2, \tag{2.20}$$

where

$$\kappa_z = (T - T_C)\kappa', \tag{2.21}$$

both κ and κ' were constant, and $k_\perp$ and k_z were reduced wave vector components perpendicular and parallel to the direction of the modulation wave, respectively. On the

other hand, the dispersion relation for optical phason is given by [2]

$$\omega^2 = \omega_{\phi C}^2 + \kappa\left[k_\perp^2 + (k_z - \pi/b)^2\right], \tag{2.22}$$

where $\omega_{\phi C}$ is a commensurate phason gap and inter-soliton distance b increases with temperature decrease as

$$b \cong b_0(1 - T_C/T)^{-1/2}, \tag{2.23}$$

if fluctuation of phase solitons is taken into account[]. Substituting the fluctuation-dissipation relation [2]

$$\chi''(k,\omega_L) = \frac{\Gamma\omega_L}{(\omega^2 - \omega_L^2)^2 + \Gamma^2\omega_L^2} \tag{2.24}$$

into eq. (2.7), $(T_{1\phi})_{ac}^{-1}$ and $(T_{1\phi})_{op}^{-1}$ are represented by [2]

$$(T_{1\phi})_{ac}^{-1} \propto \frac{\pi}{2\sqrt{2}\kappa_\perp}\sqrt{\frac{\Gamma}{\kappa_z\omega_L}} \tag{2.25}$$

and

$$(T_{1\phi})^{-1}_{op} \propto \frac{\pi}{2\sqrt{2}} \kappa^{-3/2} \sqrt{\frac{\Gamma}{\omega_L}}, \tag{2.26}$$

respectively, in the case of $\omega_\phi \langle\langle \omega_L$. Using eqs. (2.21) and (2.25), the contribution from the acoustic phason in the multi-soliton limit can be written as [2]

$$(T_{1\phi})^{-1}_{ac} \propto \left[\omega_L (T - T_C)\right]^{-1/2}, \tag{2.27}$$

in the limiting frequency region of $\omega_\phi \langle\langle \omega_L$. Equation (2.27) induced by the dispersion relation of the acoustic phason mode [2] indicates that this mode softens with approaching to some lower temperature T_C. On the other hand, $(T_{1\phi})^{-1}_{op}$ is also proportional to $1/\sqrt{\omega_L}$ but temperature independent [2]. In the opposite limiting case, $\omega_\phi \rangle\rangle \omega_L$, $T_{1\phi}^{-1}$ is also frequency independent in multi-soliton model.

2.2.2 ^{133}Cs NMR spectrum

• *Quadrupolar Perturbed NMR Spectrum*

Nuclei with spin $I > 1/2$ have electric quadrupole moments eQ. This quadrupole moment interacts with the electric field gradient around the nucleus and the quadrupolar interaction Hamiltonian $\hat{H}_Q$ is represented as [18]

$$\hat{H}_Q = \frac{eQ}{2I(2I-1)h} I \cdot \tilde{V} \cdot I, \tag{2.28}$$

where $\tilde{V}$ is the electric field gradient (EFG) tensor at the nucleus in question. If the principle axis (X, Y, Z) diagonalizing the EFG tensor is chosen, eq. (2.28) can be rewritten as

$$\hat{H}_Q = \frac{e^2 Qq/h}{4I(2I-1)} \left\{ 3I_z^2 - I(I+1) + \frac{1}{2}\eta(I_+^2 + I_-^2) \right\}, \tag{2.29}$$

where I_Z, I, I_+ and I_- mean the nuclear spin angular momentum operator along Z-axis, the nuclear spin, the raising and lowering operators, respectively. The electric field gradient eq and the asymmetric parameter η are represented by using diagonalized components of tensor V_{ij} as follows:

$$|V_{ZZ}| \geq |V_{XX}| \geq |V_{YY}|$$

$$eq = V_{ZZ}$$

$$\eta = \frac{V_{XX} - V_{YY}}{V_{ZZ}}, \quad 0 \le \eta \le 1,$$

When the external magnetic field direction is given by polar coordinates (θ, ϕ) in the principle coordination system, the 1st order perturbed quadrupolar NMR frequency $\nu_m^{(1)}$ for the transition $m \Leftrightarrow m$ -1 is represented by [19]

$$\nu_m^{(1)} = -\frac{\nu_Q}{2}\left(3\cos^2\theta - 1 + \eta\sin^2\theta\cos 2\phi\right)\left(m - \frac{1}{2}\right), \tag{2.30}$$

where

$$\nu_Q = \frac{3e^2Qq/h}{2I(2I-1)}, \tag{2.31}$$

and e^2Qq/h are called the quadrupole coupling constant [19]. In a powder specimen, the coordinates θ and ϕ are randomly distributed. The typical NMR powder pattern for ^{133}Cs with I =7/2 is illustrated in Fig. 2. 4.

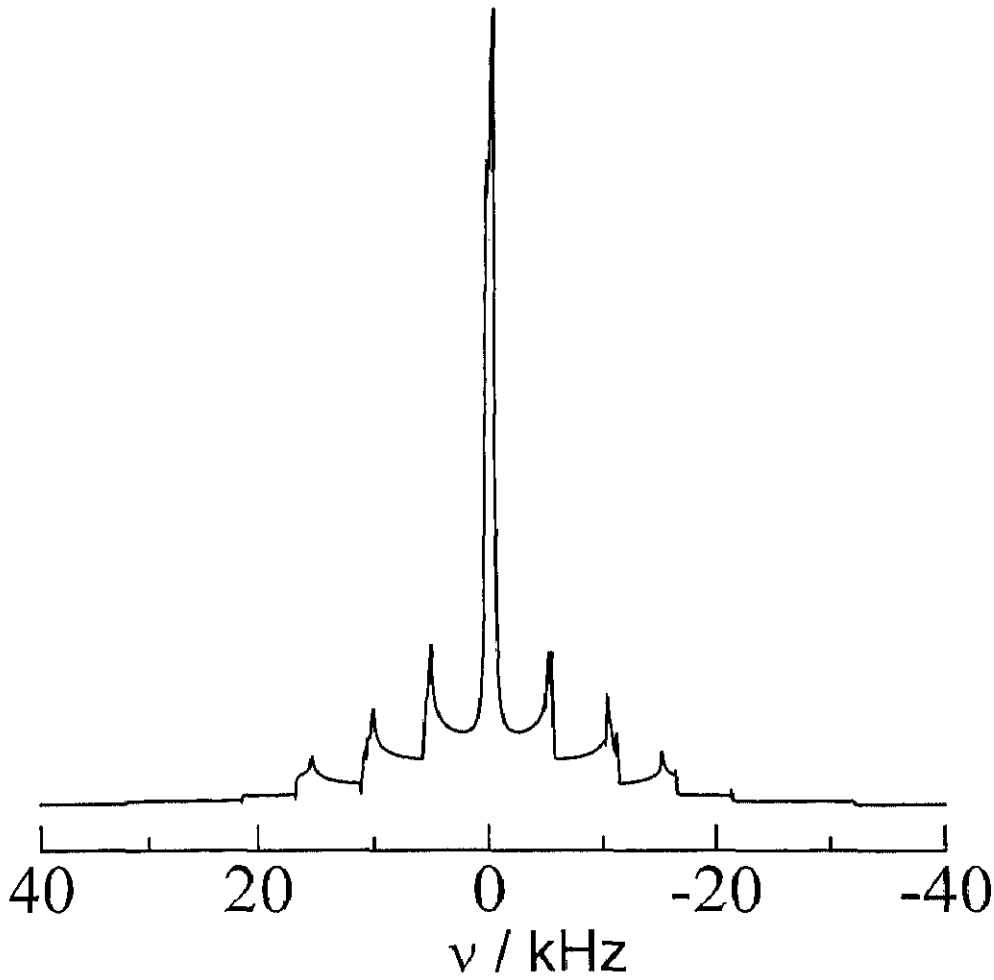

Fig. 2. 4 A typical NMR powder pattern for ^{133}Cs with $I = 7/2$. Here, the quadrupole interaction constant $e^2Qq/h = 150$ kHz and asymmetric parameter $\eta = 0.04$ are assumed.

• ^{133}Cs *NMR Lineshape in the Incommensurate phase*

In the IC phase, the characteristic NMR lineshape due to the distribution of the electric field gradient caused by the IC modulation appears [2, 20]. The lineshape $f(\nu)$ with the distribution of resonance frequencies is given by [20, 21]

$$f(\nu) \propto \left(\frac{d\nu}{dx}\right)^{-1} = \left(\frac{\partial \nu}{\partial u}\frac{\partial u}{\partial x}\right)^{-1}, \tag{2.32}$$

where $u(x)$ is the local displacement from the equilibrium position of high-temperature phase. At first, the IC modulation without the phase fluctuation is considered. The resonance frequency ν can be expanded by the powers of u

$$\nu = \nu_0 + a_1 u + a_2 u^2 + \cdots, \tag{2.33}$$

where ν_0 is the resonance frequency just above the phase transition temperature. In the plane wave limit u (x) can be represented as

$$u(x) \propto \cos(q_{IC} x). \tag{2.34}$$

By requirement from symmetry, the frequency dependence on u (eq. (2.33)) is classified in two cases.

i) linear case

The frequency variations $\delta\nu = \nu - \nu_0$ is antisymmetric against the displacement u.

In this case, the resonance frequency is governed by the linear term

$$\nu \cong \nu_0 + a_1 u = \nu_0 + \nu_1 \cos(q_{IC} x).$$

ii) quadratic case

$\delta\nu$ is symmetric and the constant a_1 must be zero. The resonance frequency is represented by

$$\nu \cong \nu_0 + a_2 u^2 = \nu_0 + \nu_2 \cos^2(q_{IC} x).$$

The resulting lineshapes are shown in Fig. 2. 5. As shown in Fig. 2. 5, the resonance line shows two edge singularities with the splitting width $\Delta\nu$ which is expected to be related to the amplitude of the IC modulation. Furthermore, considering the phase fluctuation of the IC modulation, the lineshapes become as shown in Fig. 2. 6 [20]. When the phase fluctuation of the IC modulation fulfills the fast motion regime and the frequency variation is govern by the linear term of u, the splitting width is represented by $\Delta\nu \propto (T_{IC} - T)^{\beta}$ and $\Delta\nu \propto (T_{IC} - T)^{2\beta}$ by the quadratic term, where β is the critical exponent of the IC modulation amplitude. In the slow motion regime, the temperature dependence of $\Delta\nu$ is also represented by similar formulas for the quadratic term dominant case:

$$\Delta\nu \propto (T_{IC} - T)^{\bar{\beta}} \tag{2.35}$$

where the critical exponent $\bar{\beta}$ is given by $\bar{\beta} = 2 - \alpha - \phi$, in which α is the specific heat exponent and ϕ is the crossover exponent associated with a uniaxial perturbation [22].

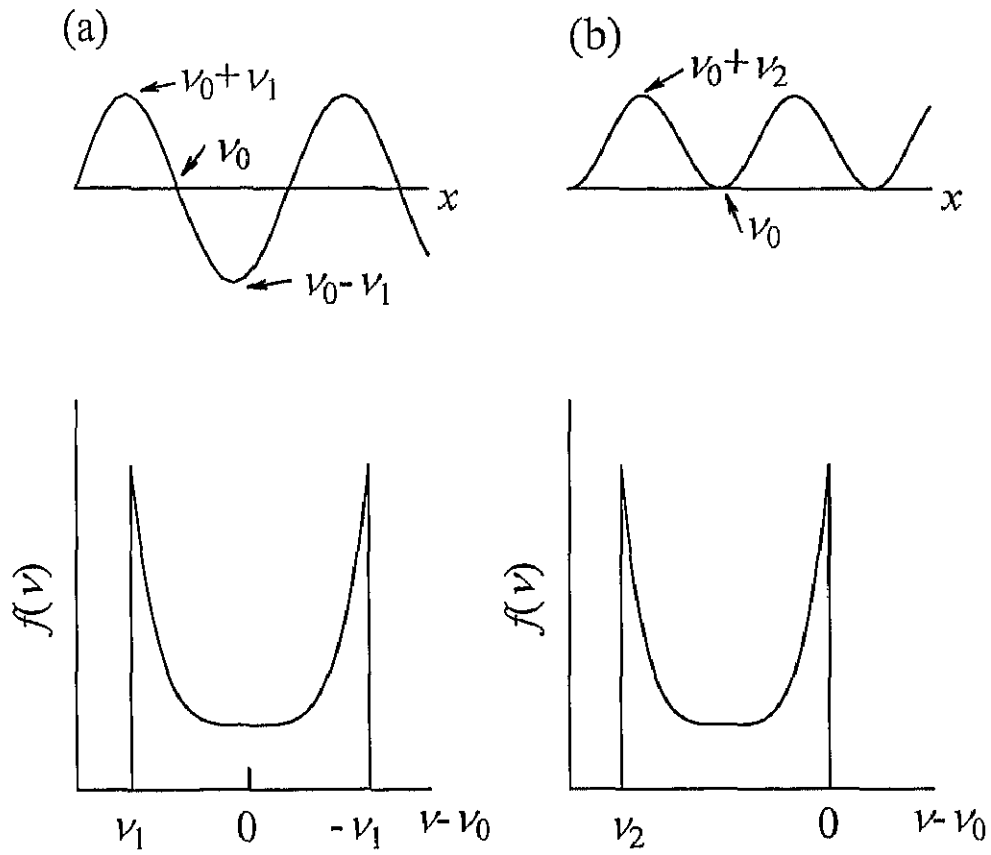

Fig. 2. 5 One-dimensional distributions of the local resonance frequency in the linear (a) and the quadratic (b) cases of the IC modulations (upper) and the corresponding resonance lineshaps $f(\nu)$, where ν_0 is the resonance frequency in the N phase.

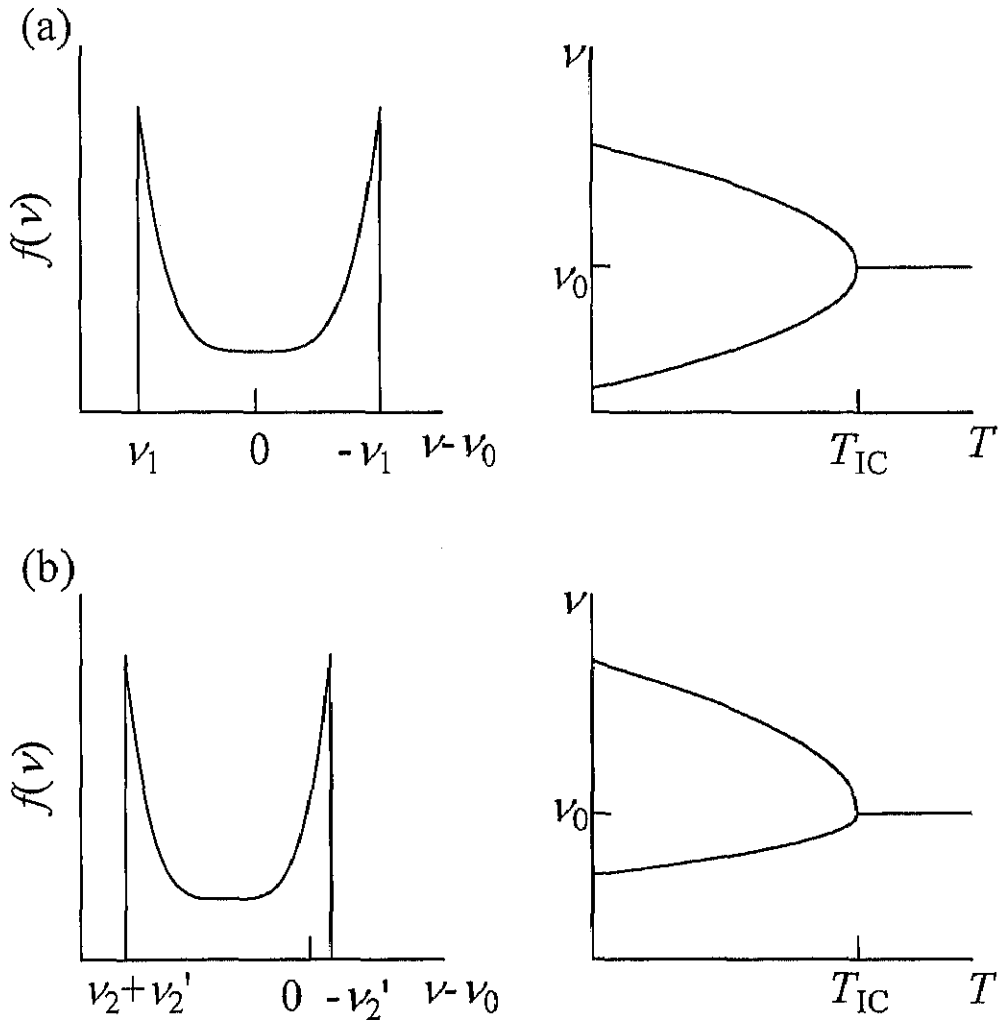

Fig. 2. 6 NMR line-shapes $f(\nu)$ and temperature dependences of splitting of resonance frequency ν in case of taking account into the phase fluctuation of the IC modulation for the linear (a) and the quadratic (b) cases, where ν_0 is the resonance frequency in the N phase.

2.3 *Cesium tetrabromocadmate Cs_2CdBr_4*

2.3.1 Introduction

The IC phase in Cs_2CdBr_4 is characterized by the modulation wave vector $q_{IC} \approx 0.15a^*$, and the IC-C transition occurs at $q_C = 0$ leading to the C phase with a structure $P2_1/n$ with $Z = 4$ (Fig. 2. 7) [23]. The modulation in the IC phase was clarified to be described by a rotational wave of the complex anion around the a axis with an amplitude of *ca.* 7° from the ^{87}Br NQR spectrum [24] and X-ray diffraction [25] measurements. The phase transition sequence observed on heating of this compound was reported as [26],

$$\underset{\substack{(P\bar{1})\\ Z=4}}{\text{commensurate}} \xrightarrow[T_{C'} = 156\ \text{K}]{} \underset{\substack{(P2_1/n)\\ Z=4}}{\text{commensurate}} \xrightarrow[T_C = 237\ \text{K}]{} \underset{(P_{1ss}^{Pnma})}{\text{incommensurate}} \xrightarrow[T_{IC} = 252\ \text{K}]{} \underset{\substack{(Pnma)\\ Z=4}}{\text{normal}}$$

where the transition temperature from the IC to the high-temperature normal (N) phase above the IC phase is given by T_{IC}. Softening of an elastic constant at the N-IC transition in Cs_2CdBr_4 has been observed by the ultrasonic measurement [27-29]. No softening of vibrational mode was, however, detected by the measurement of Raman scattering in Cs_2CdBr_4. This suggests that the N-IC-C transitions occurs by a low-angle rotational order-disorder of tetrahedral $CdBr_4^{2-}$ complex anions which couples with the translational displacement of Cs cations [27].

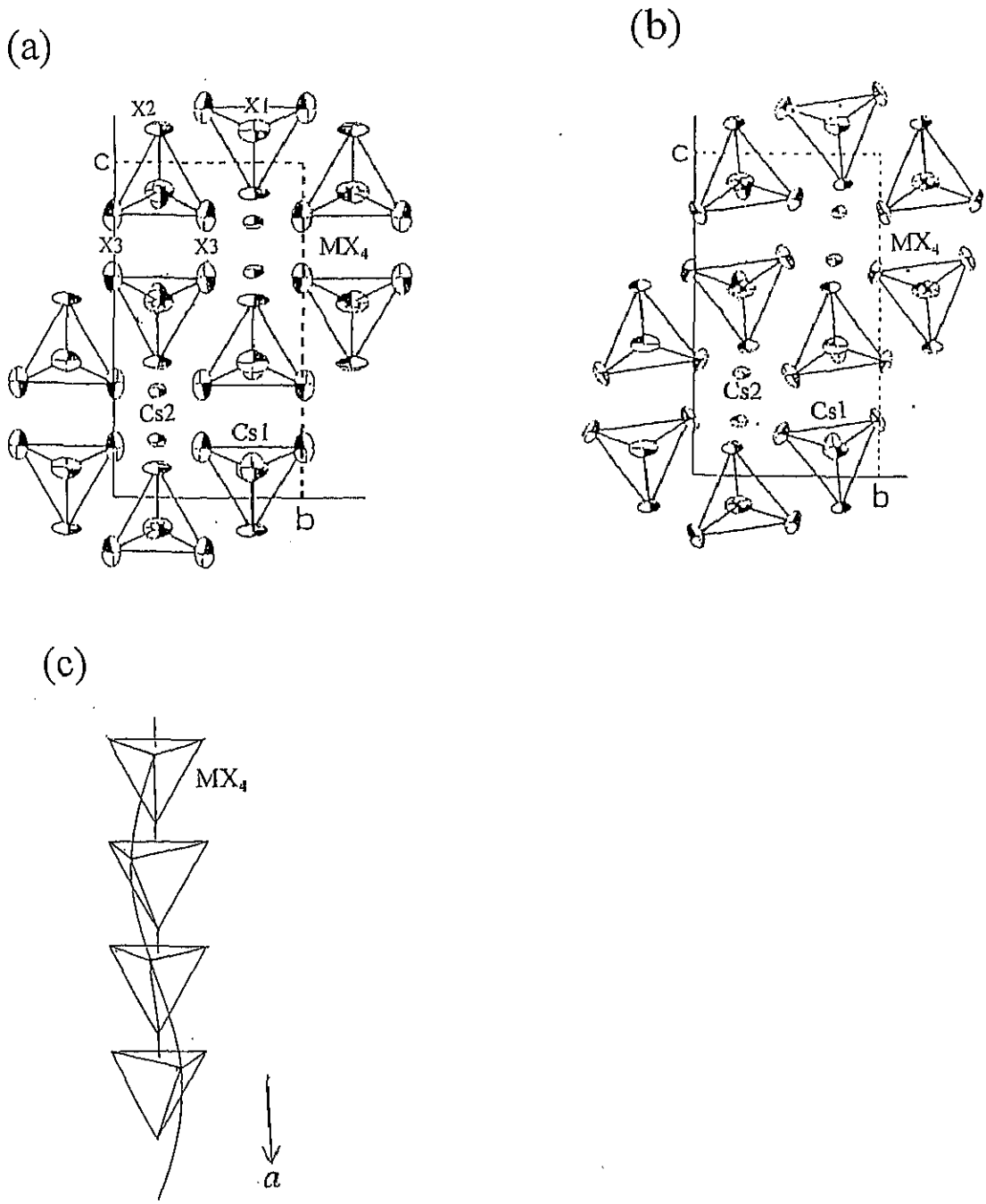

Fig. 2. 7 Crystal structures in the N phase with the space group *Pnma* ($Z = 4$) (a) and C phase with $P2_1/n$ ($Z = 4$) (b) projected on *bc*-plane and (c) the IC modulation along *a*-axis.

2.3.2 Experimental

Cs_2CdBr_4 crystal were grown by cooling a melted mixture containing stoichiometric amounts of CsBr (purity 99.9%) and $CdBr_2$ (purity 99.9%) purchased from Wako Pure Chemical Industries, Ltd. The obtained crystalline powder was dried *in vacuo* and then sealed in glass sample tubes with nitrogen gas for DTA and NMR measurements.

Differential thermal analysis (DTA) was carried out to confirm reported phase transitions in a range 100-300 K. The sample temperature was determined within ± 0.2 K by using a chromel-constantan thermocouple. X-ray powder diffraction was measured to confirm lattice parameters and determine those temperature dependence using a Phillips X'Pert PW3050/00 diffractmeter in the range 180-360 K.

The ^{133}Cs NMR spectra were measured by using a Bruker MSL-300 NMR system at a Larmor frequency of 39.4 MHz in a range 225-359 K. A saturated CsCl aqueous solution was used as a standard of frequency shift and for the preparation of the 90° pulse width. All ^{133}Cs NMR spectra obtained from FID signals observed by adding a single detection 90° pulse with the width 4-6 μs. ^{133}Cs NMR T_1 measurements were also performed with a Bruker MSL-300 NMR system using the saturation-τ- 90° pulse sequence in the range 207-369 K and also with a Bruker MSL-400 NMR system at 52.5 MHz in 245-250 K to obtain the frequency dependence of T_1. The sample temperature was controlled within ± 0.5 K by a Bruker VT-1000 temperature controller and determined by a copper-constantan thermocouple with the same accuracy. The uncertainty in the T_1 measurement was estimated to be within 5 %.

2.3.3 Results

DTA thermograms measured on heating showed endothermic anomalies due to phase transitions at 157±1, 237.3±0.6 and 252.4±0.7 K in good agreement with previously reported phase transition temperatures [26] $T_{C'}$, T_C and T_{IC}, respectively. It was confirmed from this result that crystals used in the present study formed N, IC and C phases in temperature regions $T>T_{IC}$, $T_{IC}>T>T_C$ and $T<T_C$, respectively.

An X-ray powder diffraction pattern observed at *ca.* 300 K is shown in Fig. 2. 8 with the powder pattern simulation using previously reported atomic coordinates determined at room temperature [30]. Lattice parameters determined from the obtained pattern at *ca.* 300 K together with reported values [31] shown in parentheses are a =10.23 Å (10.228 Å), b =7.93 Å (7.931 Å) and c =13.97 Å (13.966 Å). Temperature dependences of lattice parameters are shown in Fig. 2. 9. Lattice parameters a, b and c, and the cube root of a unit cell volume $V^{1/3}$ decreased with temperature decreasing accompanied by a small discontinuity at T_C for b and c, and a slight dip around T_{IC} for a, b and $V^{1/3}$.

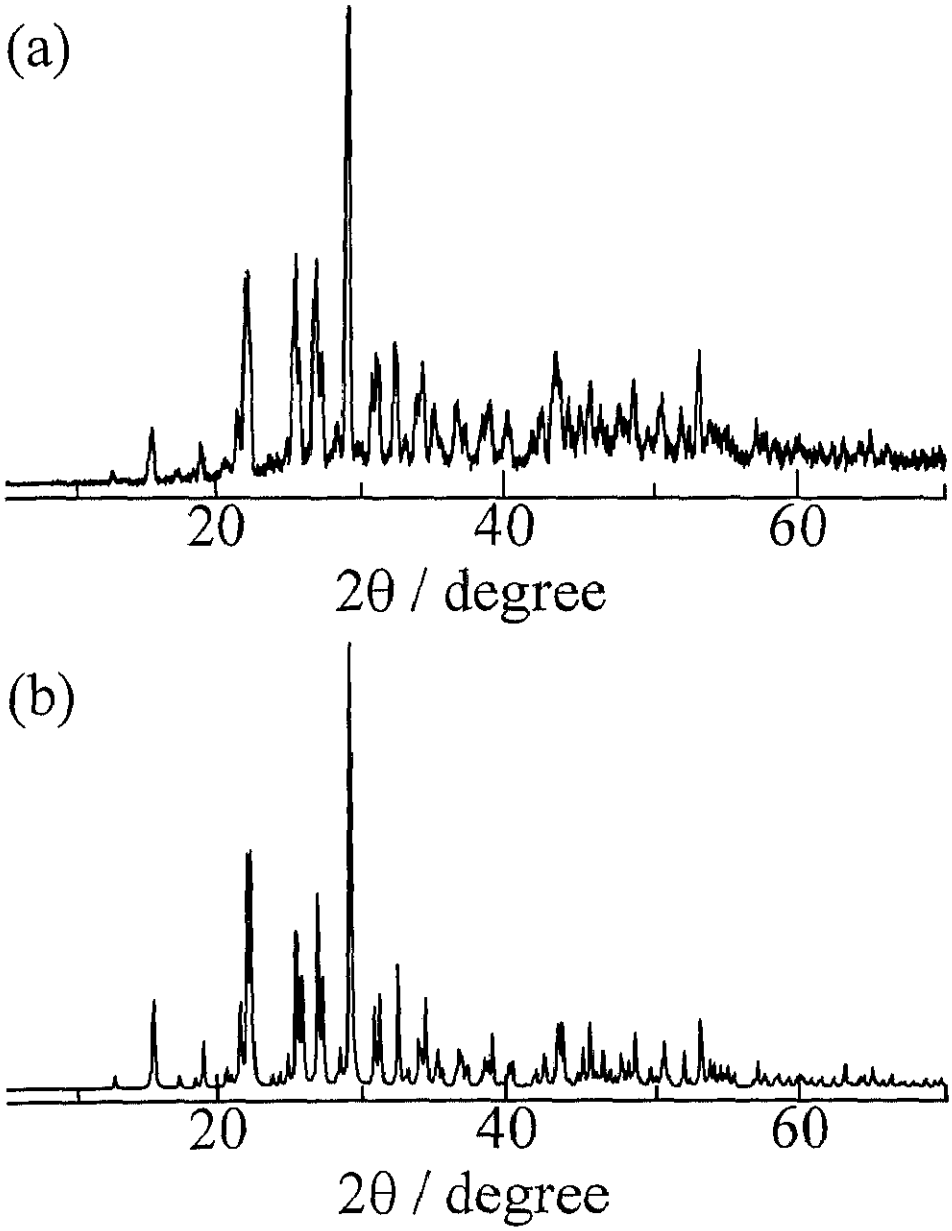

Fig. 2. 8 (a) X-ray powder diffraction pattern observed at ca. 300 K in Cs_2CdBr_4 and (b) the powder pattern simulation using the reported atomic coordinates [31].

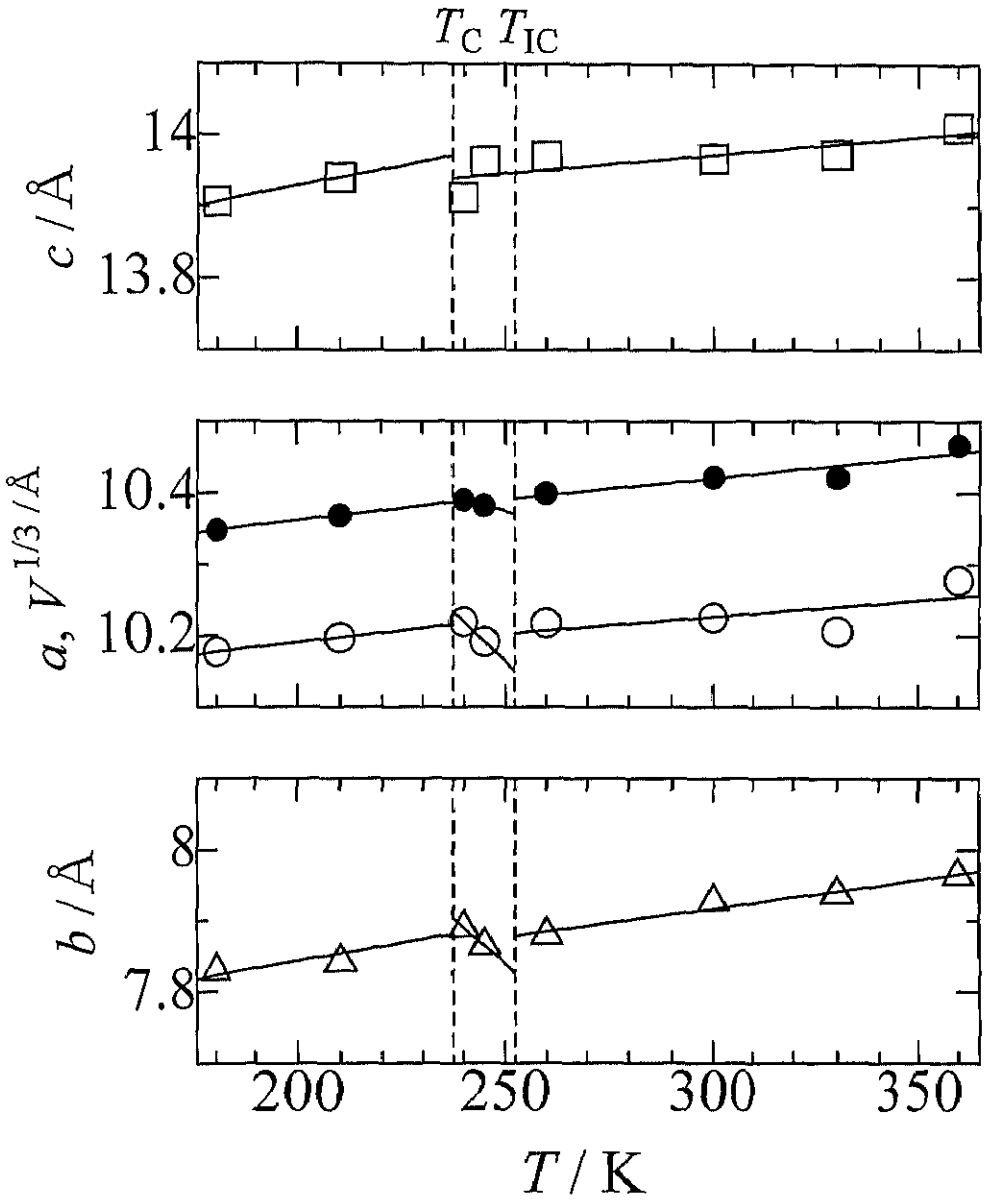

Fig. 2. 9 Temperature dependences of lattice parameters a (○), b (△) and c (□), and the cube root of a unit cell volume $V^{1/3}$ (●) in Cs_2CdBr_4.

The quadrupolar perturbed ^{133}Cs NMR spectra in the N, IC and C phases are shown in Fig. 2. 10. The width of the 90° pulse used for the measurement of powder samples was close to that for the standard CsCl aqueous solution. This suggests that all transitions in ^{133}Cs were contained in observed NMR spectra and hence ^{133}Cs nuclei have small quadrupole coupling constants (e^2Qq/h) . The line shapes were explained by the superposition of two 1st order perturbed spectra. This result is consistent with the reported crystal structure containing two nonequivalent Cs ions [30]. The quadrupole coupling constant e^2Qq/h and asymmetric parameter η for the two component were roughly estimated to be 170±40 kHz and 0.05±0.05, and 260±70 kHz and 0.5±0.2, respectively, in the N phase by referring to the values of single crystal ^{133}Cs NMR reported in Cs_2HgBr_4 (e^2Qq/h = 142.8 kHz and η = 0.04, and 271.6 kHz and 0.61) [32].

The recovery of ^{133}Cs magnetization after a 90° pulse could be reproduced by a single exponential curve in the whole temperature range yielding a single T_1 value. A temperature dependence of ^{133}Cs NMR T_1 is shown in Fig. 2. 11. The T_1 showed a discontinuous jump at T_{C1} as reported to be a 1st order phase transition. A T_1 decrease was observed around T_{IC} where a 2nd order transition was reported to take place [23]. T_1 values observed between T_{IC} and T_{C1} were shorter than those observed in the C phase and in the high temperature region of the N phase. Such shorter T_1 values can be considered to be characteristic of the IC phase [2] as described in Section 2.1.

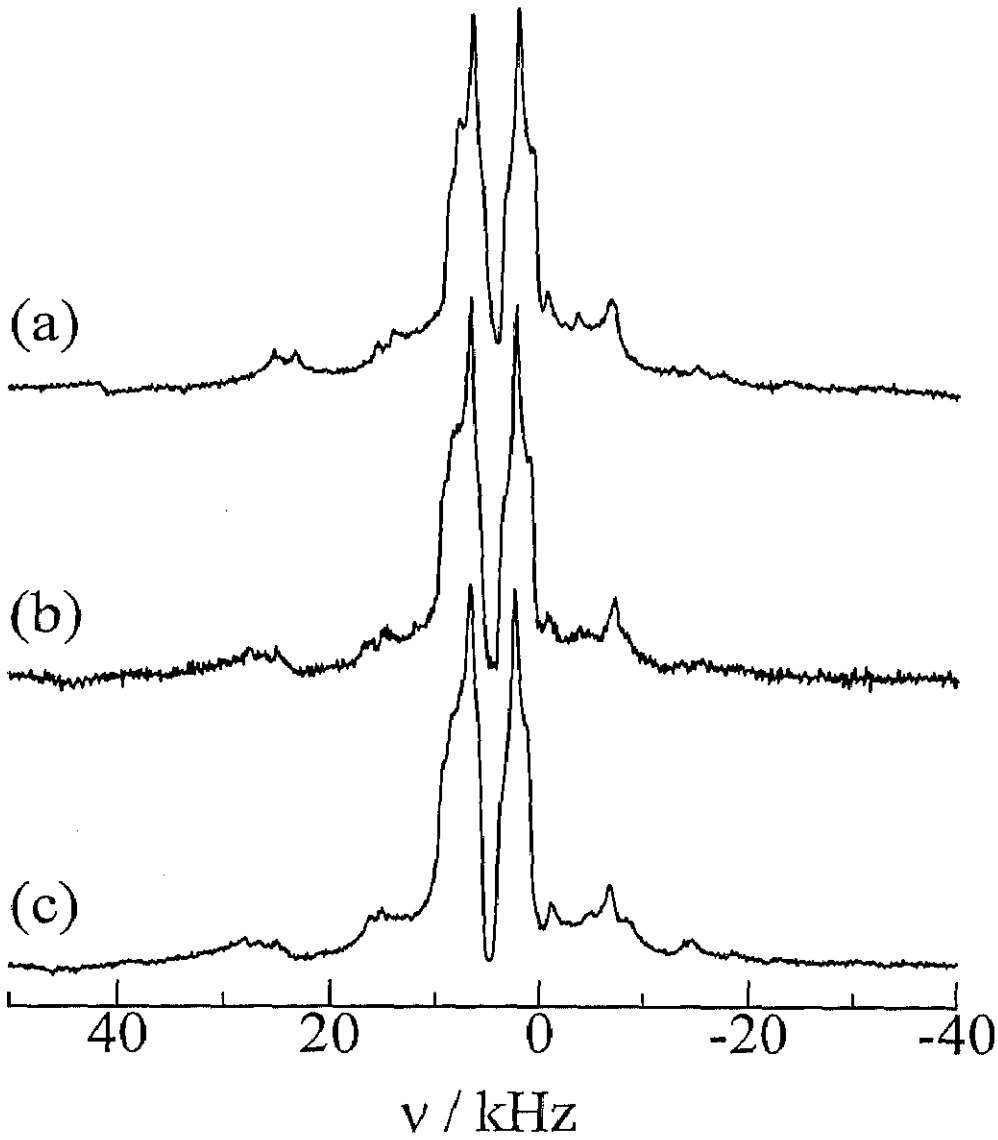

Fig. 2. 10 Quadrupolar perturbed ^{133}Cs NMR spectra measured at 39.4 MHz in the N (a), IC (b) and C phases (c) in Cs_2CdBr_4.

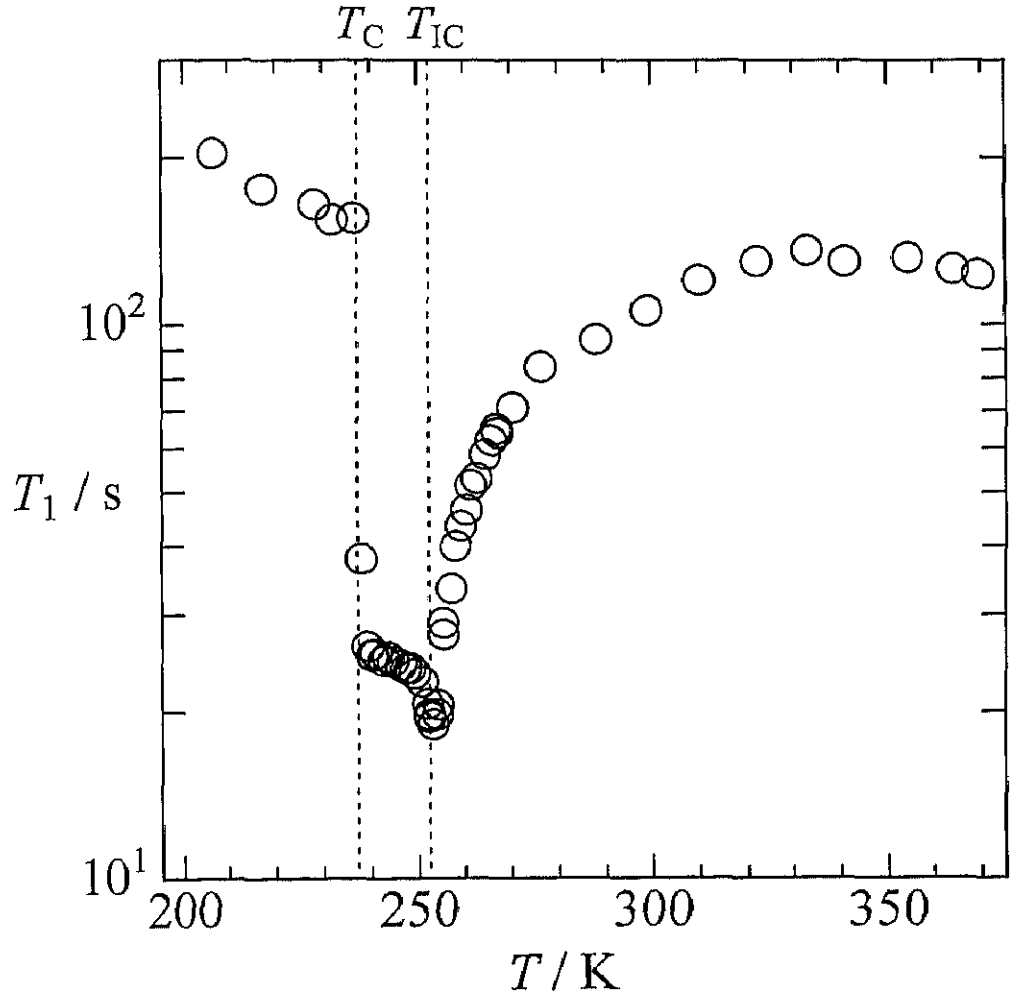

Fig. 2. 11 A temperature dependence of ^{133}Cs NMR T_1 measured at 39.4 MHz in Cs_2CdBr_4. Doted lines show the phase transition temperatures observed by DTA.

2.3.4 Discussion

The observed ^{133}Cs NMR T_1 dip in the vicinity of T_{IC} can be explained by the critical fluctuation of the quadrupole interaction due to the 2nd order phase transition. The log T_1 vs. log ε plots gave an almost straight line in the vicinity of the transition temperature $T - T_{IC} < 10$ K as shown in Fig. 2. 12. Some deviation of the best fitted line in the range $T - T_{IC} < 10$ K from the observed data with increasing temperature more than 10 K above T_{IC} can be attributed to the contribution from T_{1I} given in eq. (2.5).

The critical exponents ζ given in eq. (2.12) was determined to be 0.62 ± 0.02 from the fitting. This value agrees well with the values of $\zeta = 0.625$ predicted theoretically for the three-dimensional XY model (Table 2. 1) [33]. The theoretical treatment has predicted that the three-dimensional XY model is acceptable for the N-IC transition because the order parameter u, which represents the displacement of atom from the equilibrium position in the N phase, is represented by two components of the incommensurate modulation, i.e., the amplitude and the phase of the IC wave [33]. Many of previously reported critical exponents in N-IC transitions of A_2BX_4 family have been explained by applying this model [1].

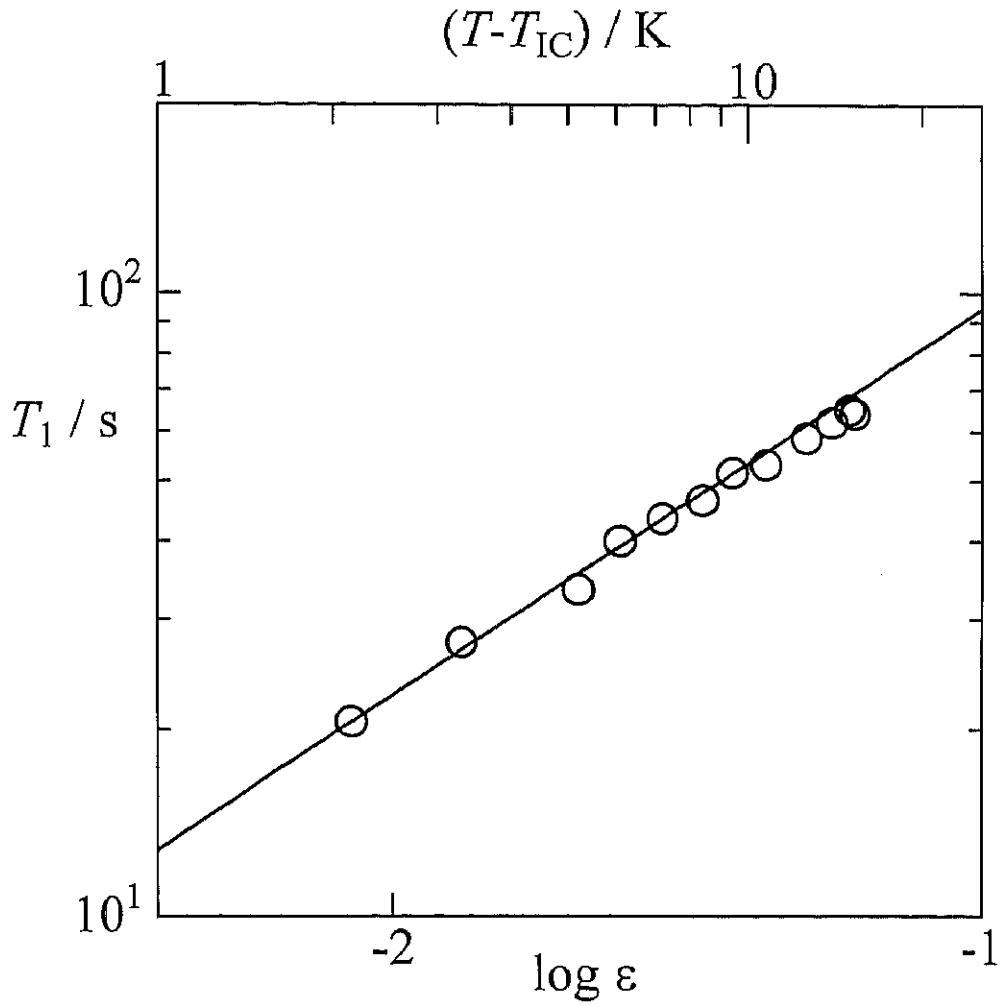

Fig. 2. 12 A critical plot of ^{133}Cs NMR T_1 above the N-IC phase transition in Cs_2CdBr_4. Solid line is the best-fitted curve using eq. (2.12) in the range of $\varepsilon = (T - T_{IC}) / T_{IC} < -1.4$.

Incommensurate (IC) phase

Marked short T_1 values were observed in the IC phase compared with those in N and C phases. Cs_2CdBr_4 showed a frequency dependent T_1 in the IC phase as shown in Fig. 2. 13. This frequency dependence of T_1 values obsered in the IC phase could be represented by a relation: $T_1 \propto \omega_L^{0.48}$. Substituting this relation of T_1 into eq. (2.15), a small phason gap $\nu_\phi = \omega_\phi / 2\pi$, 0 - 2 MHz, is derived suggesting to fulfill the condition $\omega_\phi \langle\langle \omega_L$. This agrees with the result of ^{87}Rb NMR T_1 in Rb_2ZnCl_4 studied by Misho *et al.* reporting the phason gap in the order of 10 MHz [17].

Since the IC phase gave T_1 values shorter than those in the C phase and the high-temperature range of the N phase, the contribution from usual lattice vibrations is expected to be negligible. Ignoring this contribution, the T_1 could be fitted by eqs.(2.13) - (2.16) as shown in Figs. 2. 13. In the present study, the critical exponent of the amplitudon contribution on T_1 was assumed to be the classical limit giving $\zeta' = 0.5$ [2], because the amplitudon contribution was shown to emerge only in the neighborhood of the T_{IC} and could not be separated from the total T_1. In Cs_2CdBr_4, the fitted curves could well reproduce the observed T_1 values in a wide range of the IC phase. The fitted T_1 values in the vicinity of T_C, however, became shorter than the observed values. This suggests that the IC modulation wave changes from the plane wave limit to the multi-soliton in this temperature region.

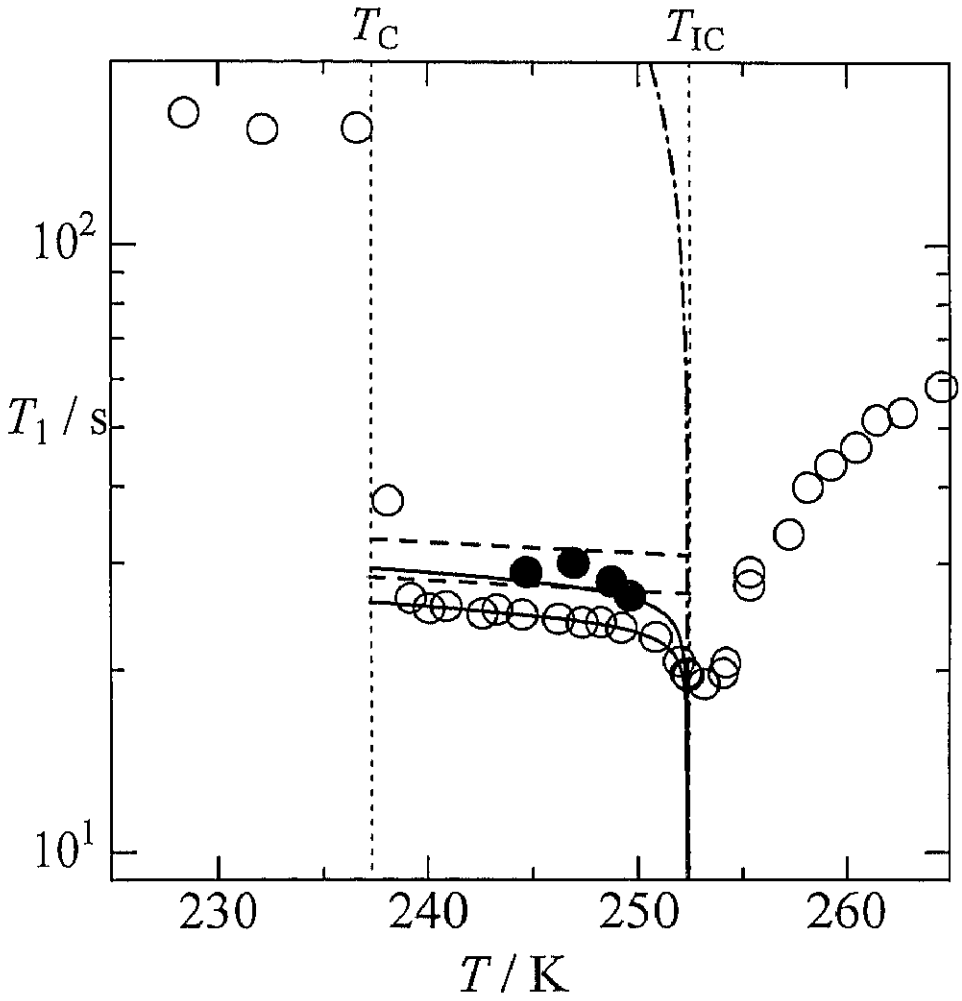

Fig. 2. 13 Temperature and frequency dependences of ^{133}Cs NMR T_1 in the IC phase of Cs_2CdBr_4 measured at 39.4 (○) and 52.5 (●) MHZ. Solid lines are the best-fitted curves calculated by introducing phason (broken lines) and amplitudon (chain line) contributions. Vertical doted lines correspond to phase transition temperatures observed by DTA.

Commensurate (C) phase

From the theoretical consideration [2], we can anticipate that, since the phase of the commensurate modulation in C phase is locked, the modulation can no more slide freely and the phason becomes a normal lattice mode. This results in a discontinuous increase of T_1 at T_C in agreement with the observed result.

2.4 Cesium tetrabromomercurate Cs_2HgBr_4

2.4.1 Introduction

The IC phase in Cs_2HgBr_4 is characterized by the modulation wave vector $q_{IC} \approx 0.15a^*$, and IC-C transitions occurs at $q_C = 0$ leading to the C phase with $P2_1/n$ with $Z = 4$ same as Cs_2CdBr_4 crystal [23]. The modulation in the IC phase was clarified to be described by rotational wave of the complex anion around the a axis with an amplitude of *ca.* 7° from the ^{87}Br NQR spectrum measurement [24]. The phase transition sequence observed on heating was reported as [34]

	$T_{C''} = 84$ K		$T_{C'} = 165$ K		$T_C = 230$ K		$T_{IC} = 243$ K	
commensurate	→	commensurate	→	commensurate	→	incommensurate	→	normal
$(P\bar{1})$		$(P\bar{1})$		$(P2_1/n)$		(P_{1ss}^{Pnma})		$(Pnma)$
$Z = 8$		$Z = 4$		$Z = 4$				$Z = 4$

where the transition temperature from the IC to the high-temperature normal (N) phase above the IC phase is given by T_{IC}. No softening of vibrational mode was detected by the measurement of Raman scattering [35]. This suggests that the N-IC-C transitions are

occured by low-angle rotational order-disorder of tetrahedral $HgBr_4^{2-}$ complex anions which couples with the translational displacement of Cs cations [35]. Actually, the presence of disorder of the complex anion in the N phase was confirmed by the recent X-ray diffraction [36] and the Raman scattering [37] measurements in Cs_2HgBr_4.

2.4.2 Experimental

Cs_2HgBr_4 crystal was grown by cooling a melted mixture containing stoichiometric amounts of CsBr (purity 99.9%) and $HgBr_2$ (purity 99.9%) purchased from Wako Pure Chemical Industries, Ltd. The obtained crystalline powder was dried *in vacuo* and then sealed in glass sample tubes with nitrogen gas for DTA and NMR measurements.

Differential thermal analysis (DTA) was carried out to confirm the reported phase transitions in the range 100-300 K. The sample temperature was determined within ± 0.2 K by a chromel-constantan thermocouple.

X-Ray powder diffraction was measured to confirm lattice parameters and determine their temperature dependence using a Phillips X'Pert PW3050/00 diffractmeter in the range 180-360 K. The sample temperature was measured by a copper-constantan thermocouple.

The ^{133}Cs NMR spectra were measured by using a Bruker MSL-300 NMR system at a Larmor frequency of 39.4 MHz at 202-362 K. A saturated CsCl aqueous solution was used as a standard of frequency shift and for setting the width of the 90° pulse. All ^{133}Cs NMR spectra obtained from FID signals observed by adding a single detection 90° pulse with the width 4-6 μs. ^{133}Cs NMR T_1 measurements were performed with a Bruker MSL-300 NMR system at a Larmor frequency of 39.4 MHz using the

saturation-τ- 90° pulse sequence in the range 197-369 K and also with a Bruker MSL-400 NMR system at 52.5 MHz in 236-241 K to obtain the T_1 frequency dependence. The sample temperature was controlled within ± 0.5 K by a Bruker VT-1000 temperature controller and determined by a copper-constantan thermocouple with the same accuracy. The uncertainty in the T_1 measurement was estimated to be within 5 %.

2.4.3 Results

DTA thermograms measured on heating showed endothermic anomalies due to phase transitions at 164.5 ± 1.0, 231.1 ± 0.6 and 243.8 ± 0.7 K in good agreement with previously reported phase transition temperatures $T_{C'} = 243$ K, $T_C = 230$ K and $T_{IC} = 165$ K [23], respectively. It was confirmed from this result that crystals used in the present study formed N, IC and C phases in temperature regions $T > T_{IC}$, $T_{IC} > T > T_C$ and $T < T_C$, respectively.

An X-ray powder diffraction pattern observed at *ca.* 300 K is shown in Fig. 2. 14 with a pattern simulated with previously reported atomic coordinates determined at 295 K [36]. Lattice parameters determined from the obtained pattern at *ca.* 300 K together with reported values in parentheses are a =10.33 Å (10.248 Å), b =7.92 Å (7.927 Å) and c =13.92 Å (13.901 Å). Temperature dependences of lattice parameters are shown in Fig. 2. 15. The lattice length b decreased upon cooling with a small gap at T_C. a, c and $V^{1/3}$ displayed slight dips around T_{IC}. Furthermore, a increased with temperature decrease down to *ca.* 300 K and showed a maximum around 300 K. $V^{1/3}$ showed a plateau above *ca.*300 K.

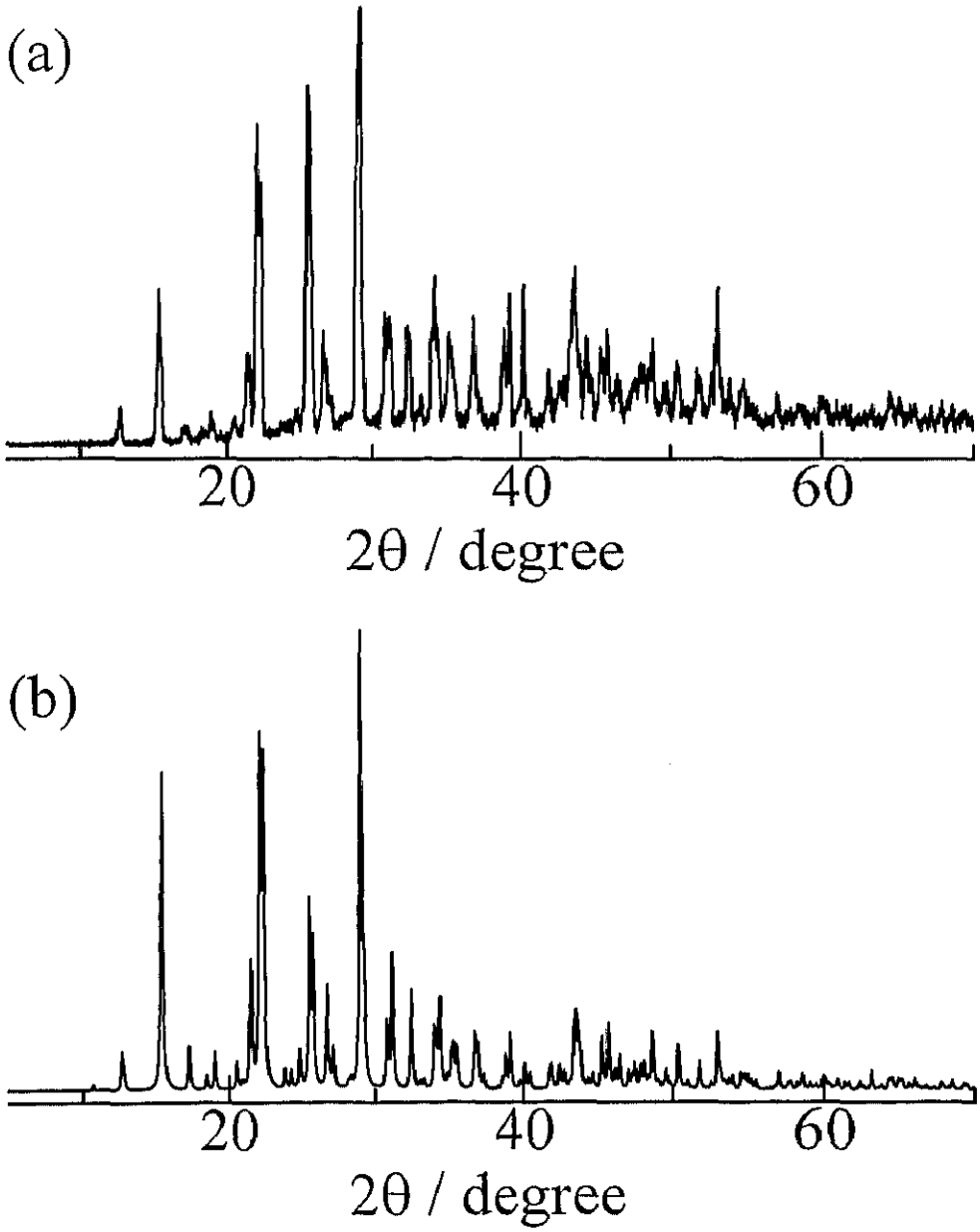

Fig. 2. 14 (a) An X-ray powder diffraction pattern observed at ca. 300 K in Cs_2HgBr_4. (b) A simulated powder pattern using reported atomic coordinates [36].

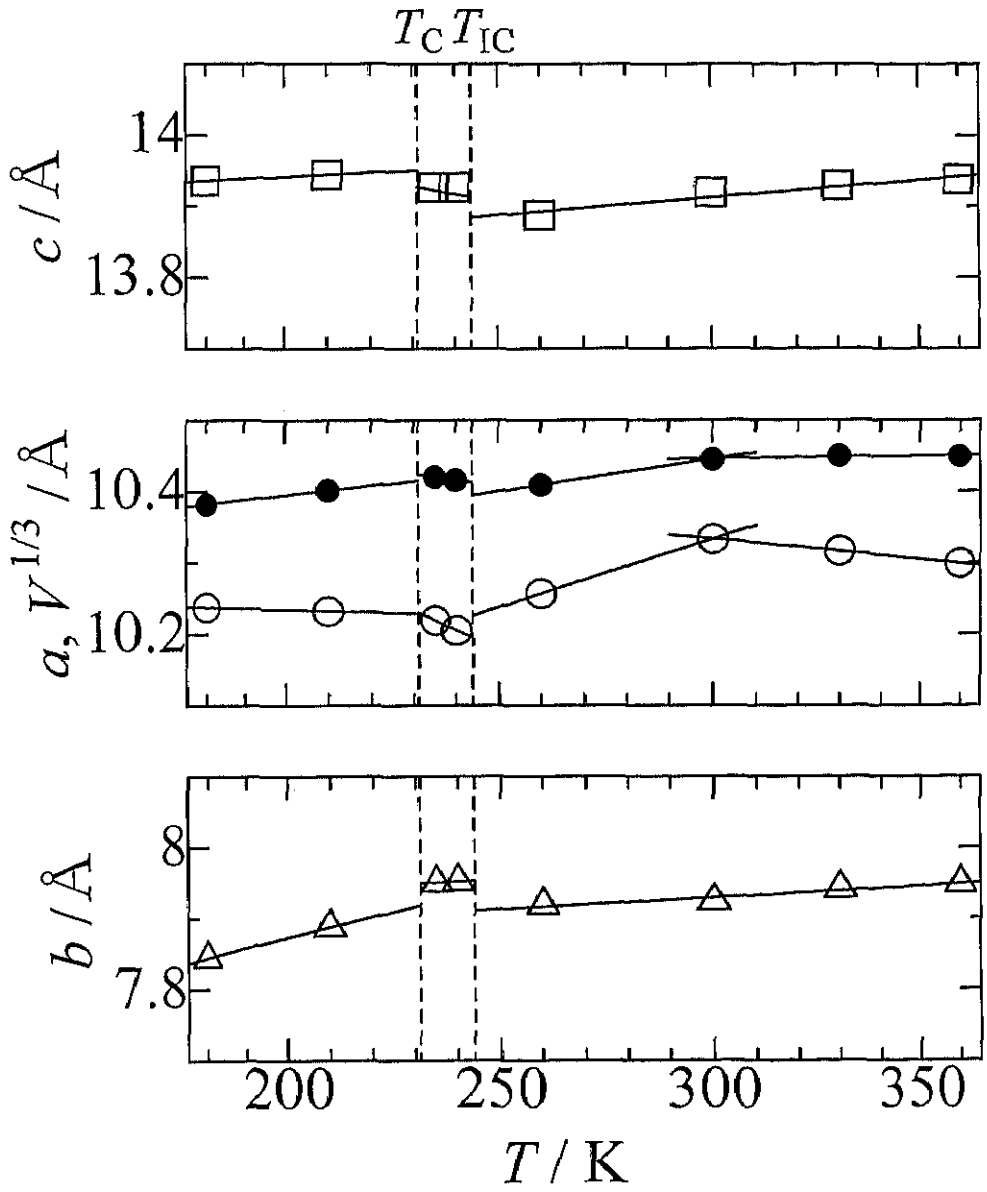

Fig. 2. 15 Temperature dependences of lattice parameters a (○), b (△) and c (□), and the cube root of a unit cell volume $V^{1/3}$ (●) in Cs_2HgBr_4.

The quadrupolar perturbed ^{133}Cs NMR spectra in the N, IC and C phases are shown in Fig. 2. 16. The width of the 90° pulse tuned for measurement of powdered Cs_2HgBr_4 was close to that for a standard CsCl aqueous solution. This suggests that all single quantum transitions in ^{133}Cs NMR in Cs_2HgBr_4 crystal were contained in the observed spectra, i.e., ^{133}Cs nuclei have small e^2Qq/h in this compound. The line shapes were explained by the superposition of two 1st order perturbed spectra. This result is consistent with the reported crystal structure containing two nonequivalent Cs ions [36]. The e^2Qq/h and η were estimated to be 150 ± 30 kHz and 0.05 ± 0.05, and 280 ± 40 kHz and 0.6 ± 0.1, respectively, in the N phase for Cs_2HgBr_4. These obtained values agree well with the values obtained in the single crystal ^{133}Cs NMR measurement in Cs_2HgBr_4 [32].

Since the recovery of ^{133}Cs magnetization could be reproduced by a single exponential curve in the whole temperature range, a single T_1 could be determined. Temperature dependences of ^{133}Cs NMR T_1 are shown in Fig. 2. 17. The T_1 showed a discontinuous jump at T_{C1} where a 1st order phase transition was reported. T_1 decrease was observed around T_{IC} being reported to be a 2nd order transition temperature [23]. T_1 values observed between T_{IC} and T_{C1} were shorter than those in the C phase and high temperature region of the N phase. Such short T_1 values are characteristic of the IC phase [2].

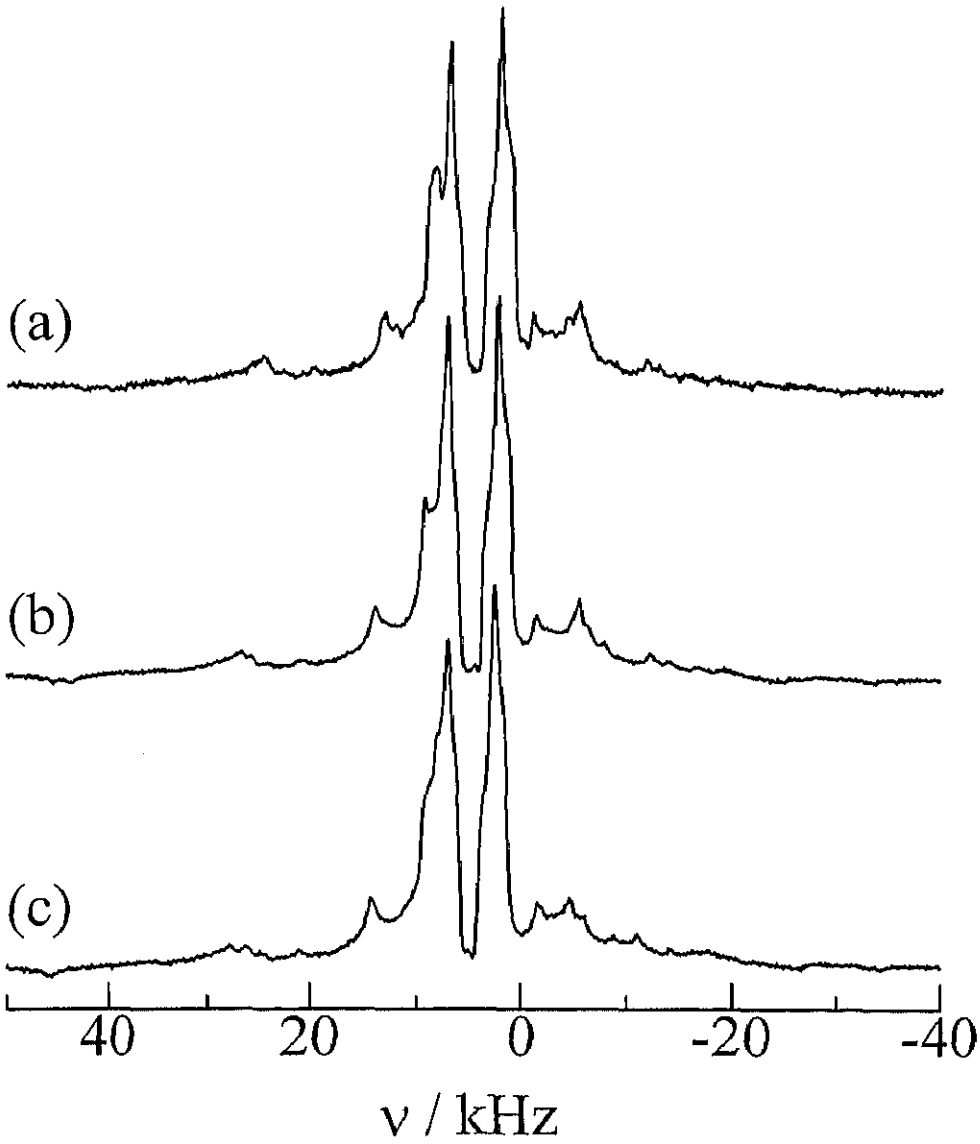

Fig. 2. 16 Quadrupolar perturbed ^{133}Cs NMR spectra measured at 39.4 MHz in the N (a), IC (b) and C phases (c) in Cs_2HgBr_4.

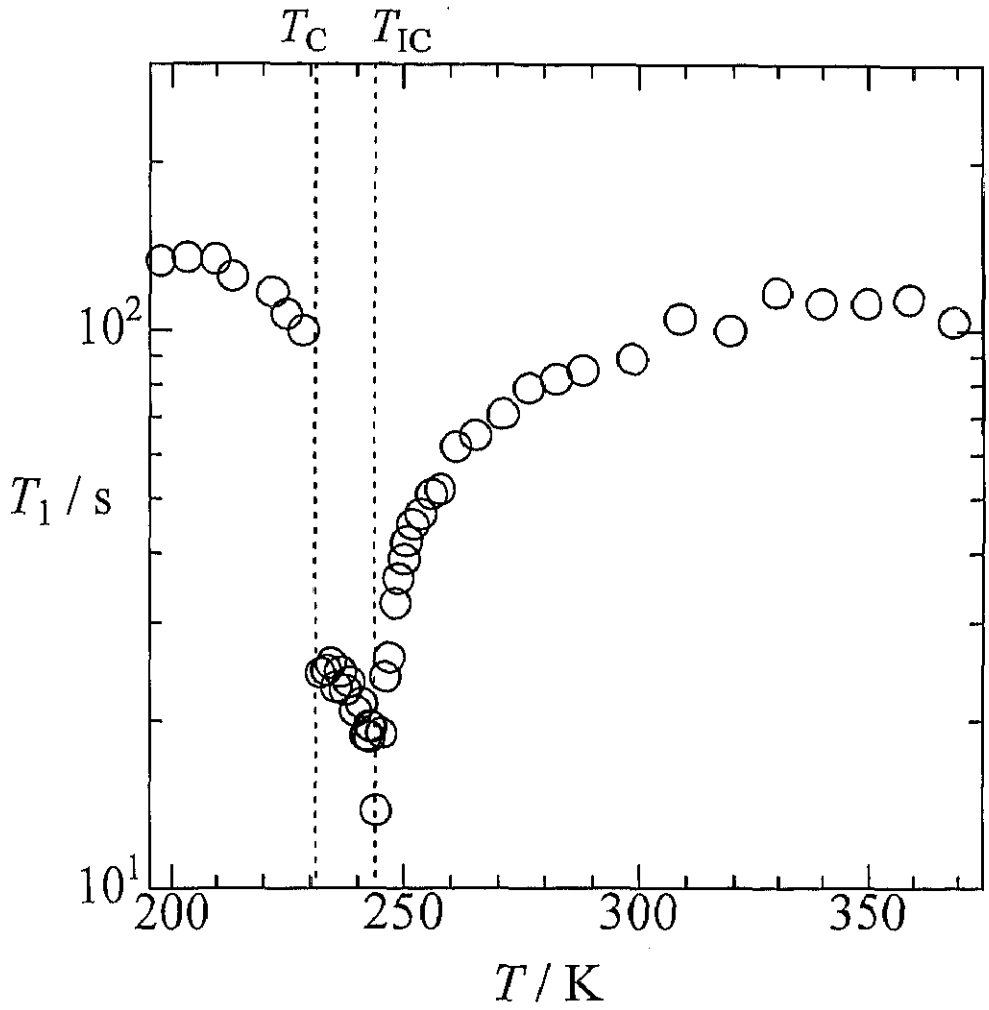

Fig. 2. 17 A temperature dependence of ^{133}Cs NMR T_1 measured at 39.4 MHz in Cs_2HgBr_4. Doted lines show the phase transition temperatures observed by DTA.

2.4.4 Discussion

Normal (N) phase

The observed ^{133}Cs NMR T_1 dip in the vicinity of T_{IC} can be explained by the critical fluctuation of the quadrupole interaction due to the instability of the lattice near the 2nd order phase transition. The log T_1 vs. log ε plots gave an almost straight line in the vicinity of the transition temperature as shown in Fig. 2. 18. The plots in Cs_2HgBr_4 also showed some deviation of the straight line from the observed values due to the contribution from T_{1l} given in eq. (2.5)with increasing temperature.

The critical exponent ζ given in eq. (2.12) was determined to be 0.50 ± 0.02 K. This value agrees well with $\zeta = 0.5$ calculated for the classical mean field approximation [4]. This result is consistent with the previously reported critical exponent $\beta = 0.5$ [32], which supports the mean field theory, derived from a single crystal ^{133}Cs NMR spectrum measurement in Cs_2HgBr_4. The classical exponent obtained in Cs_2HgBr_4 is a rare case because many of previously reported critical exponents in N-IC transitions of A_2BX_4 family have been explained by applying three-dimensional *XY* model [1]. This result suggests that the interionic interaction works in the long range in Cs_2HgBr_4 crystal.

Incommensurate (IC) phase

Marked short T_1 values observed in the IC phase compared with those in N and C phases. Cs_2HgBr_4 also showed a frequency dependent T_1 in the IC phase as shown in Fig. 2. 19. The frequency dependence of T_1 in the IC phase could be represented by a relation $T_1 \propto \omega_L^{0.41}$. Substituting this frequency dependence of T_1 into eq. (2.15), a

small phason gap $\nu_\phi = \omega_\phi / 2\pi$, 0 - 8 MHz, is derived. This can be considered to roughly fulfill the condition $\omega_\phi \langle\langle \omega_L$.

Ignoring the contribution from usual lattice vibrations, the T_1 was fitted by using eqs.(2.13)-(2.16) as shown in Fig. 2. 19, where the critical exponents $\zeta' = 0.5$ [2] was assumed for Cs_2HgBr_4 also. The fitted curve could well reproduce the observed T_1 values in a wide range of the IC phase. In contrast to Cs_2CdBr_4, the fitted values in Cs_2HgBr_4 showed no marked deviation from the T_1 value observed even at the region close to T_C, as shown in Fig. 2. 19, suggesting the absence of multi-soliton behavior in Hg complex. This result agrees with the previously reported ^{133}Cs NMR spectrum measurement of Cs_2HgBr_4 single crystal [32]. This fact that the IC modulation in Cs_2HgBr_4 crystal could be explained by a continuous sinusoidal plane wave down to near the IC-C transition implies that the interionic interaction works over long range, i.e., a mean field approximation is probably fulfilled in this system. This may be concerned closely with the fact that the critical exponent ζ at the N-IC phase transition in the N phase side coincides with the value of the mean field approximation in Cs_2HgBr_4.

Commensurate (C) phase

In the C phase, ^{133}Cs T_1 is governed by normal lattice vibration. The observed T_1 was longer than in IC phase and the high temperature regone in N phase, and showed a moderate dependence on temperature. No anomaly was observed in all temperature region observed in this phase even near the first order IC-C transition.

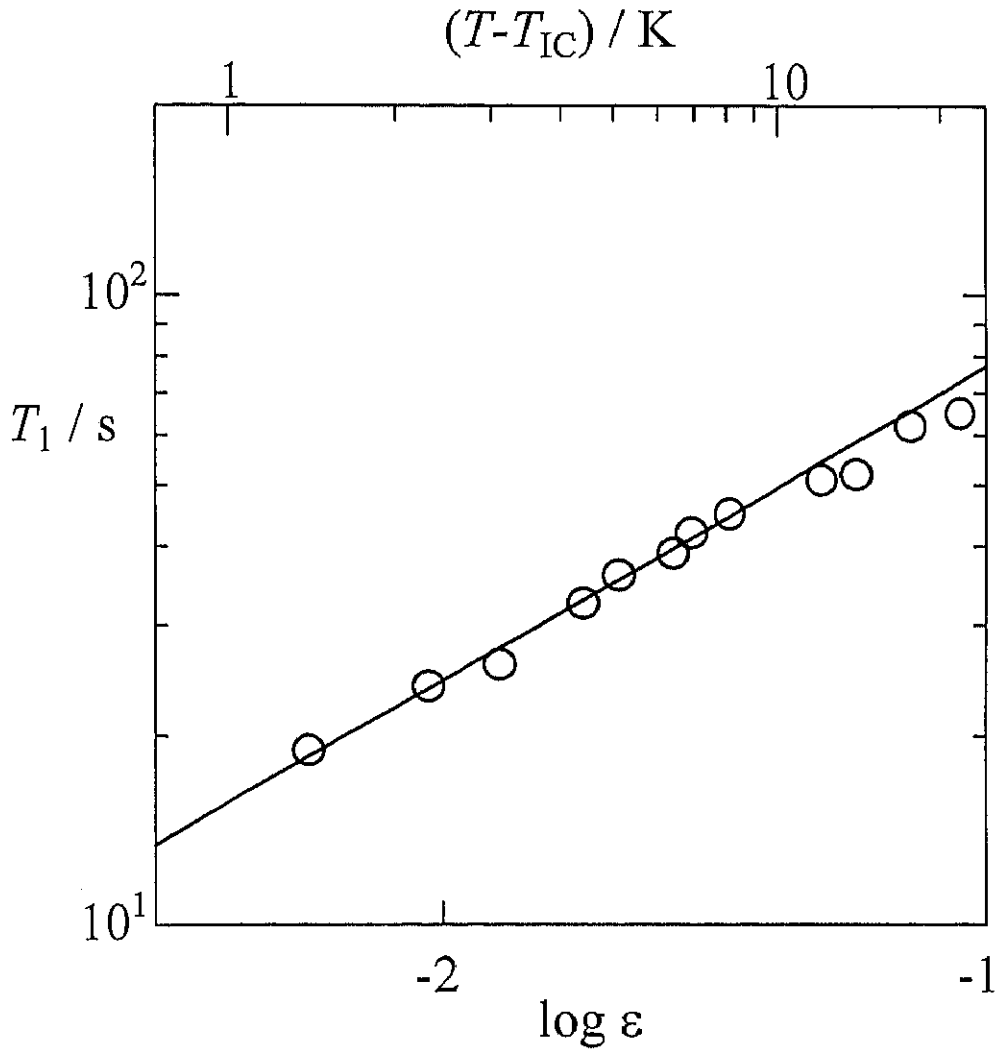

Fig. 2. 18 A critical plot of ^{133}Cs NMR T_1 above the N-IC phase transition in Cs_2HgBr_4. Solid line is the best-fitted curve using eq. (2.12) in the range of $\varepsilon = (T - T_{IC}) / T_{IC} < -1.4$.

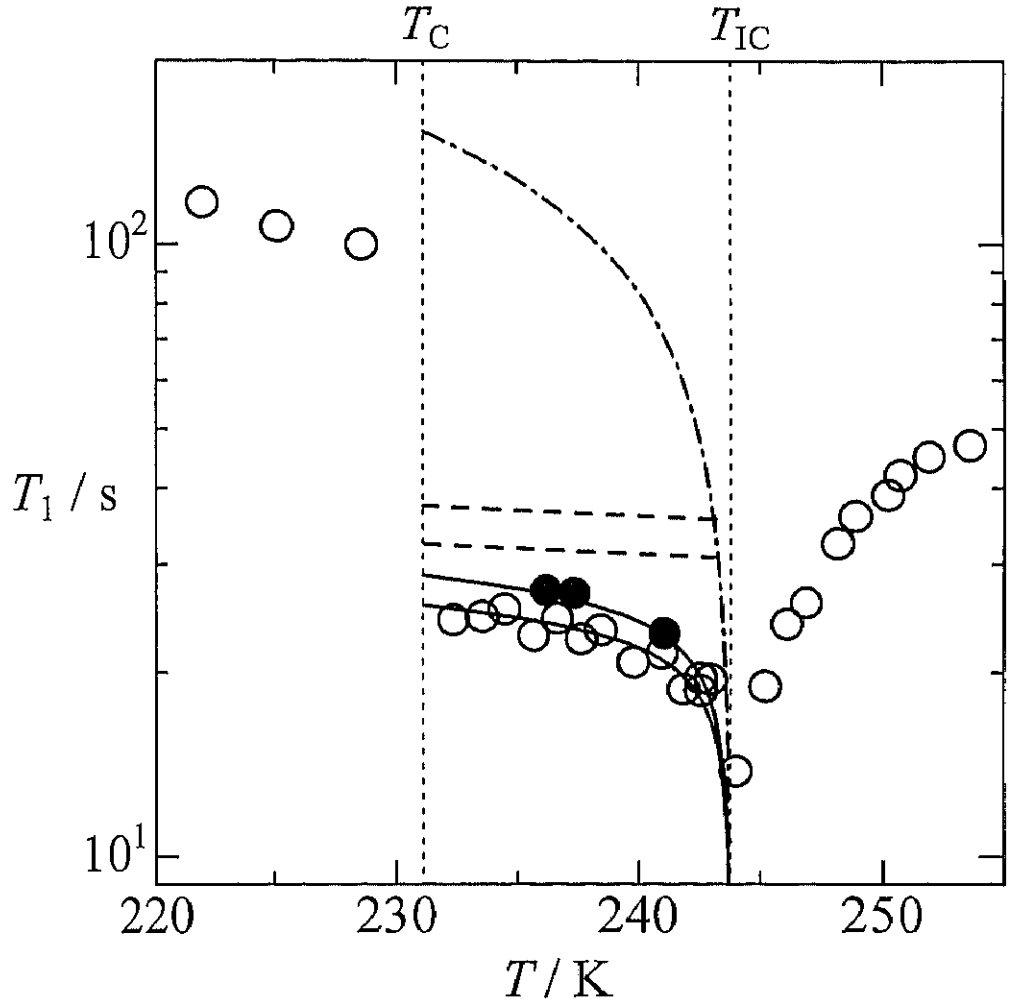

Fig. 2. 19 Temperature and frequency dependences of ^{133}Cs NMR T_1 in the IC phase of Cs_2HgBr_4 measured at 39.4 (○) and 52.5 (●) MHZ. Solid lines are the best-fitted curves calculated by introducing phason (broken lines) and amplitudon (chain line) contributions. Vertical doted lines correspond to phase transition temperatures observed by DTA.

2.5 *Cesium tetraiodocadmate Cs_2CdI_4*

2.5.1 Introduction

Cs_2CdI_4 crystal has been reported to form two modifications, A and B, at room temperature depending on the condition of crystal growth [38, 39]. The modification-A, whose structure is orthorhombic *Pnma*, is obtained from a molten stoichiometric mixture of CsI and CdI_2 while the monoclinic modification-B ($P2_1/m$) crystallizes in aqueous solution[38, 39]. The modification-B undergoes no phase transition below room temperature but transforms to the modification-A at *ca.* 420 K. On the other hand, the modification-A undergoes successive phase transitions [39]:

$$\underset{\text{commensurate}}{\underset{(P\bar{1})}{\underset{Z=8}{}}} \xrightarrow[T_{C'}=183.4\text{ K}]{} \underset{\text{commensurate}}{\underset{(P2_1/n)}{\underset{Z=4}{}}} \xrightarrow[T_C=259.6\text{ K}]{} \underset{\text{incommensurate}}{\underset{(P_{1ss}^{Pnma})}{}} \xrightarrow[T_{IC}=332.3\text{ K}]{} \underset{\text{normal}}{\underset{(Pnma)}{\underset{Z=4}{}}}$$

The N and C phases in this compound are isomorphous with the corresponding phases in other Cs_2MBr_4 compounds (M = Cd, Hg)[], while a modulation wave vector in the IC phase ($q_{IC} \approx 0.26a^*$) [39] is different from the bromo compound ($q_{IC} \approx 0.15a^*$) [23].

2.5.2 Experimental

Cs_2CdI_4 crystals were grown by slow evaporation of an aqueous solution containing stoichiometric amounts of CsI and CdI_2 (both 99.9%). The obtained crystalline powder was kept *in vacuo* at 450 K in order to be transformed to the modification-A, then sealed in glass sample tubes with nitrogen gas for DTA and NMR measurements.

Differential thermal analysis (DTA) was carried out to confirm reported phase

transitions in the range 100-370 K. The sample temperature was determined within ± 0.2 K by using chromel-constantan thermocouple.

X-Ray powder diffraction was measured to confirm lattice parameters and determine their temperature dependence using a Phillips X'Pert PW3050/00 diffractmeter in the range 170-450 K for modification-A of Cs_2CdI_4 after annealing at *ca.* 450 K. The sample temperature was measured by a copper-constantan thermocouple.

The ^{133}Cs NMR spectra were measured by using a Bruker MSL-300 NMR system at a Larmor frequency of 39.4 MHz in the range 228-360 K. A saturated CsCl aqueous solution was used as a standard of frequency shift and for setting the width of the 90° pulse. All ^{133}Cs NMR spectra obtained from FID signals observed by adding a single detection 90° pulse with the width 4-6 μs. ^{133}Cs NMR T_1 measurements were performed with a Bruker MSL-300 NMR system at a Larmor frequency of 39.4 MHz using the saturation-τ- 90° pulse sequence in the range 225-373 K and also with a Bruker MSL-400 NMR system at 52.5 MHz in 266-317 K for Cs_2CdI_4 to obtain the T_1 frequency dependence. The sample temperature was controlled within ±0.5 K by a Bruker VT-1000 temperature controller and determined by a copper-constantan thermocouple with the same accuracy. The uncertainty in the T_1 measurement was estimated to be within 5 %.

2.5.3 Results

X-ray powder diffraction peaks of crystals obtained from an aqueous solution and after heat-treatment at 450 K were well explained by the reported structure [40] of modification-B and A, respectively, as shown in Figs. 2. 20 and 2. 21. In all following

experiments in this chapter, the results of the heat-treated specimens are discussed. About the experimental X-ray powder diffraction data on modification-B which has a Sr_2GeS_4 type structure are described in the next chapter. Lattice parameters determined from the experimental pattern obtained at *ca.* 450 K together with reported values at 180℃ [40] shown in parentheses are a =10.90 Å (10.914 Å), b =8.53 Å (8.565 Å) and c =14.91 Å (14.954 Å). DTA thermograms measured on heating direction displayed endothermic anomalies due to phase transitions at 183±1, 259.3±0.6 and 331.6±0.7 K in good agreement with reported phase transition temperatures $T_{C'}$ = 332.3 K, T_C = 259.6 K and T_{IC} = 183.4 K [39], respectively. It was confirmed from these results that the crystals used in the present study form N, IC and C phases in temperature regions $T > T_{IC}$, $T_{IC} > T > T_C$ and $T < T_C$, respectively. Temperature dependeences of lattice parameters of modification-A are shown in Fig. 2. 22. Here, half values of a and V at *ca.* 170 K in C' phase is also shown for comparison, because the unit cell length a below $T_{C'}$ is twice of that of the higher temperature phases. The values of a, b, c and $V^{1/3}$ above *ca.* 360K were approximately temperature independent and those in the IC phase decreased rapidly with temperature decrease. Furthermore, a below *ca.* 245 K decreased and b below *ca.* 200 K increased upon cooling.

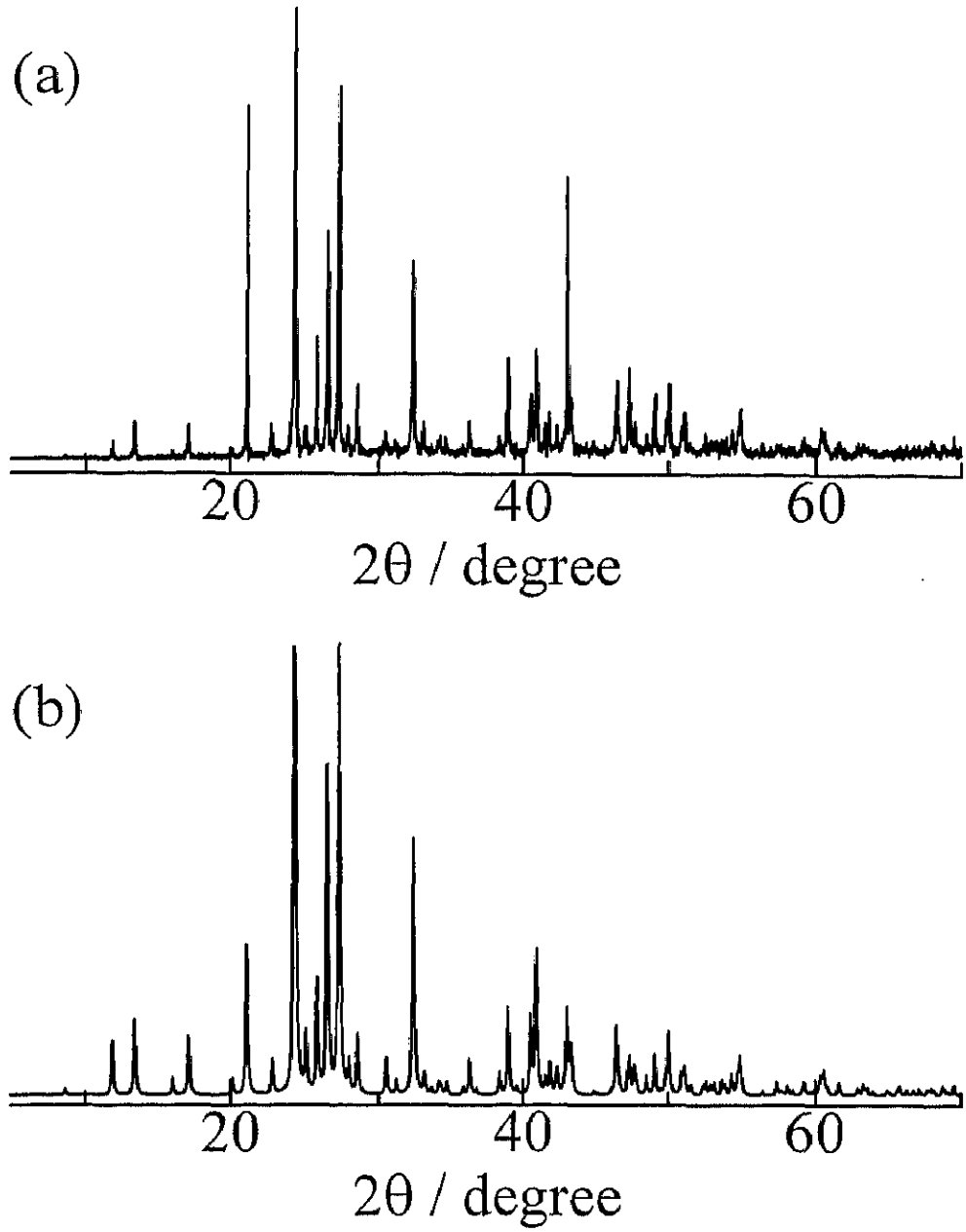

Fig. 2. 20 (a) An X-ray powder diffraction pattern observed at ca. 300 K in the modification-B of Cs_2CdI_4. (b) A simulated powder pattern using reported atomic coordinates [40].

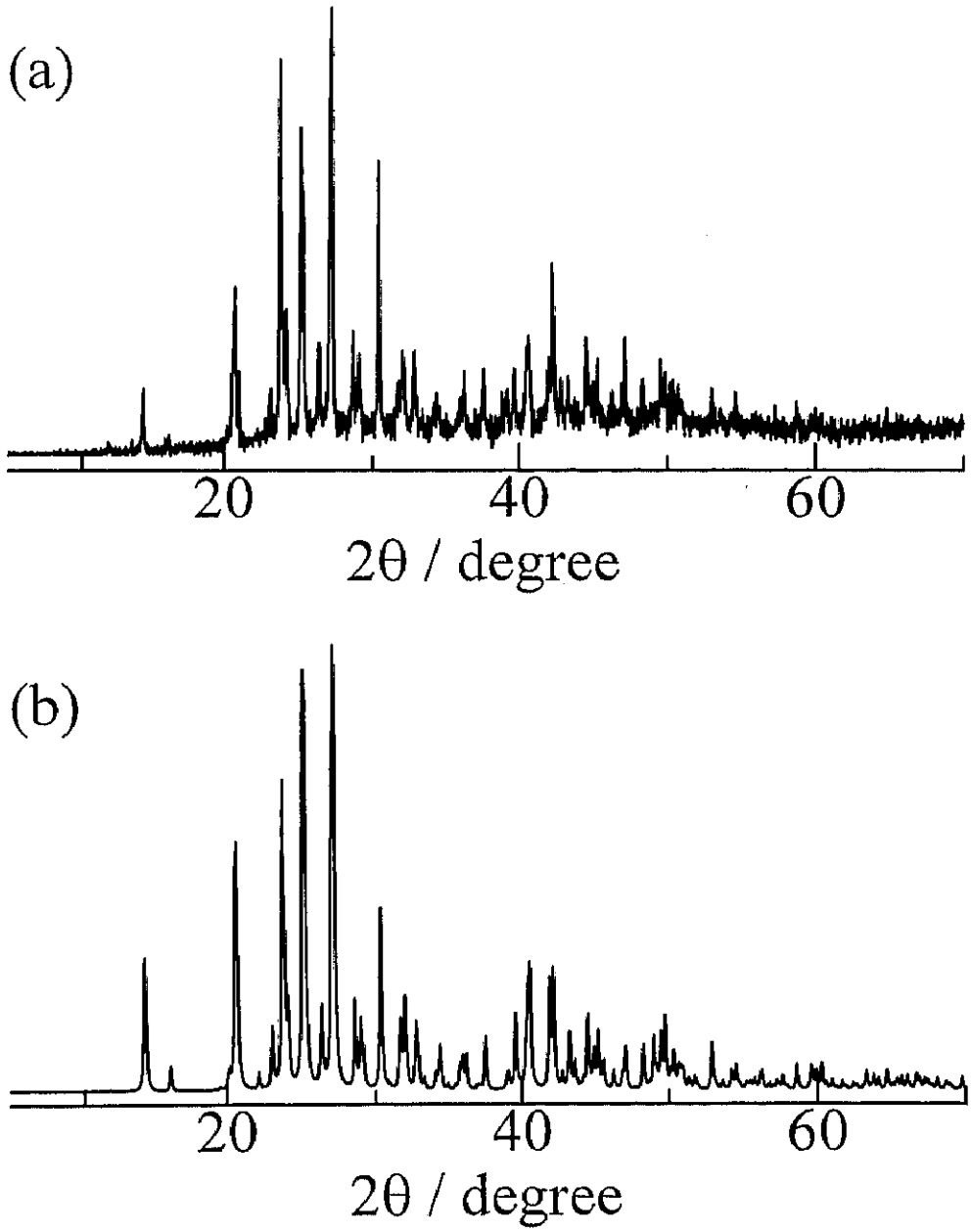

Fig. 2. 21 (a) An X-ray powder diffraction pattern observed at ca. 450 K in the modification-A of Cs_2CdI_4. (b) A simulated powder pattern using reported atomic coordinates [40].

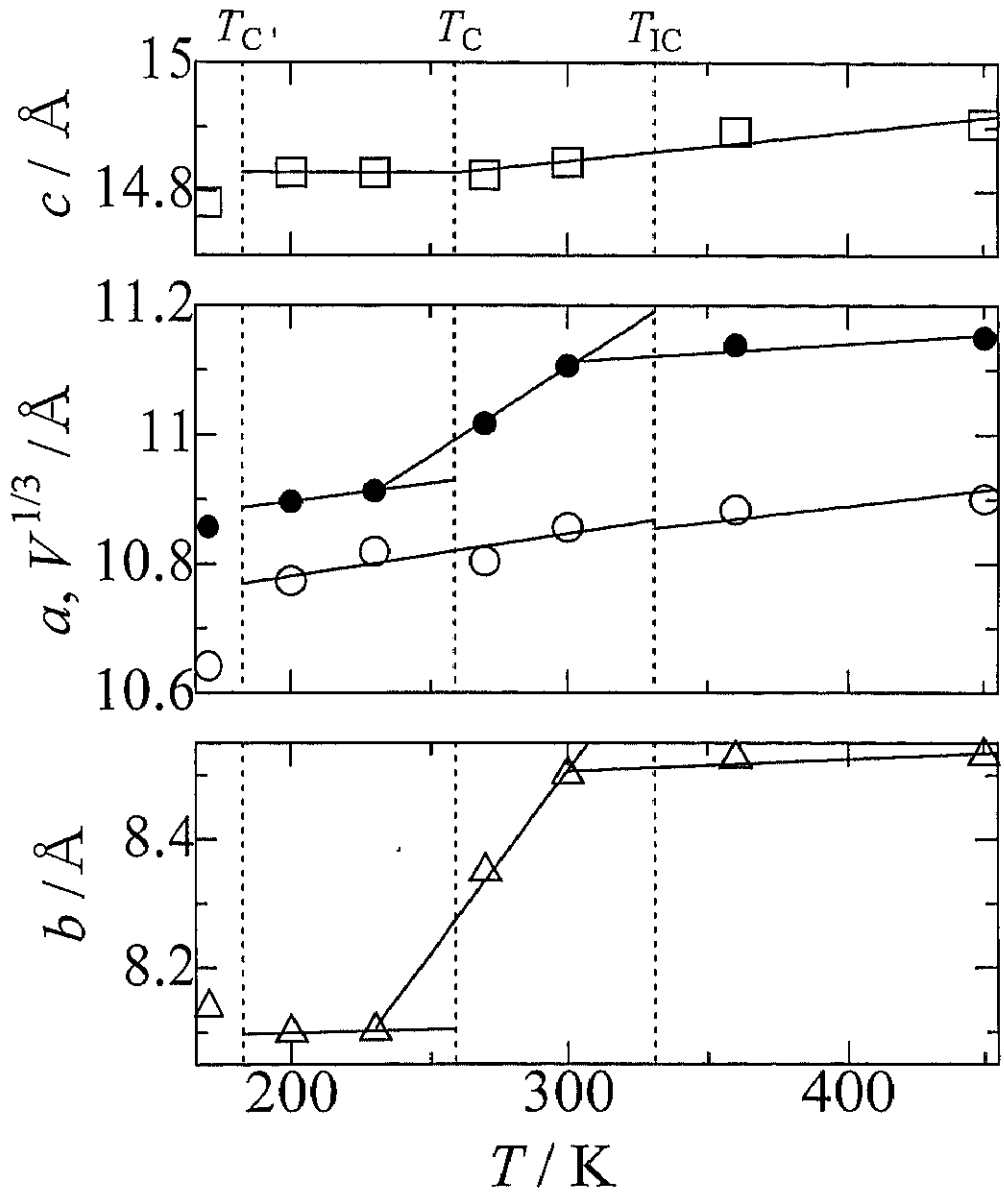

Fig. 2. 22 Temperature dependences of lattice parameters a (○), b (△) and c (□), and the cube root of a unit cell volume $V^{1/3}$ (●) in the modification-A of Cs_2CdI_4.

The quadrupolar perturbed ^{133}Cs NMR spectra in the N, IC and C phases are shown in Fig. 2. 23. The width of the 90° pulse tuned for measurement of powder samples was close to that for a standard CsCl aqueous solution. This suggests that all single quantum transitions in ^{133}Cs NMR in Cs_2CdI_4 crystal were contained in the observed spectra, i.e., ^{133}Cs nuclei have small e^2Qq/h in this compound. The line shapes can be explained by the superposition of two 1st order perturbed spectra. This result is consistent with the reported crystal structure revealing the presence of two crystallographically nonequivalent Cs ions [40]. The quadrupole coupling constant e^2Qq/h and asymmetric parameter η were roughly determined to be 150 ± 40 kHz and 0.2 ± 0.1, and 300 ± 80 kHz and 0.6 ± 0.1, respectively in the N phase by referring to the values, 142.8 kHz, 0.04, and 285.0 kHz, 0.61, obtained from the single crystal ^{133}Cs NMR measurement in Cs_2HgBr_4 [32].

Since the recovery of ^{133}Cs magnetization could be reproduced by a single exponential curve in the whole temperature range, unique T_1 values could be determined. Temperature dependences of ^{133}Cs NMR T_1 are shown in Fig. 2. 24. The T_1 showed a discontinuous jump at T_{C1} reported to be a 1st order phase transition temperature. T_1 decrease was observed around T_{IC}. T_1 values observed between T_{IC} and T_{C1} were shorter than those in the C phase and the high temperature region of the N phase, and showed a frequency dependency. Such short and frequency dependent T_1 values are characteristic in the IC phase [2].

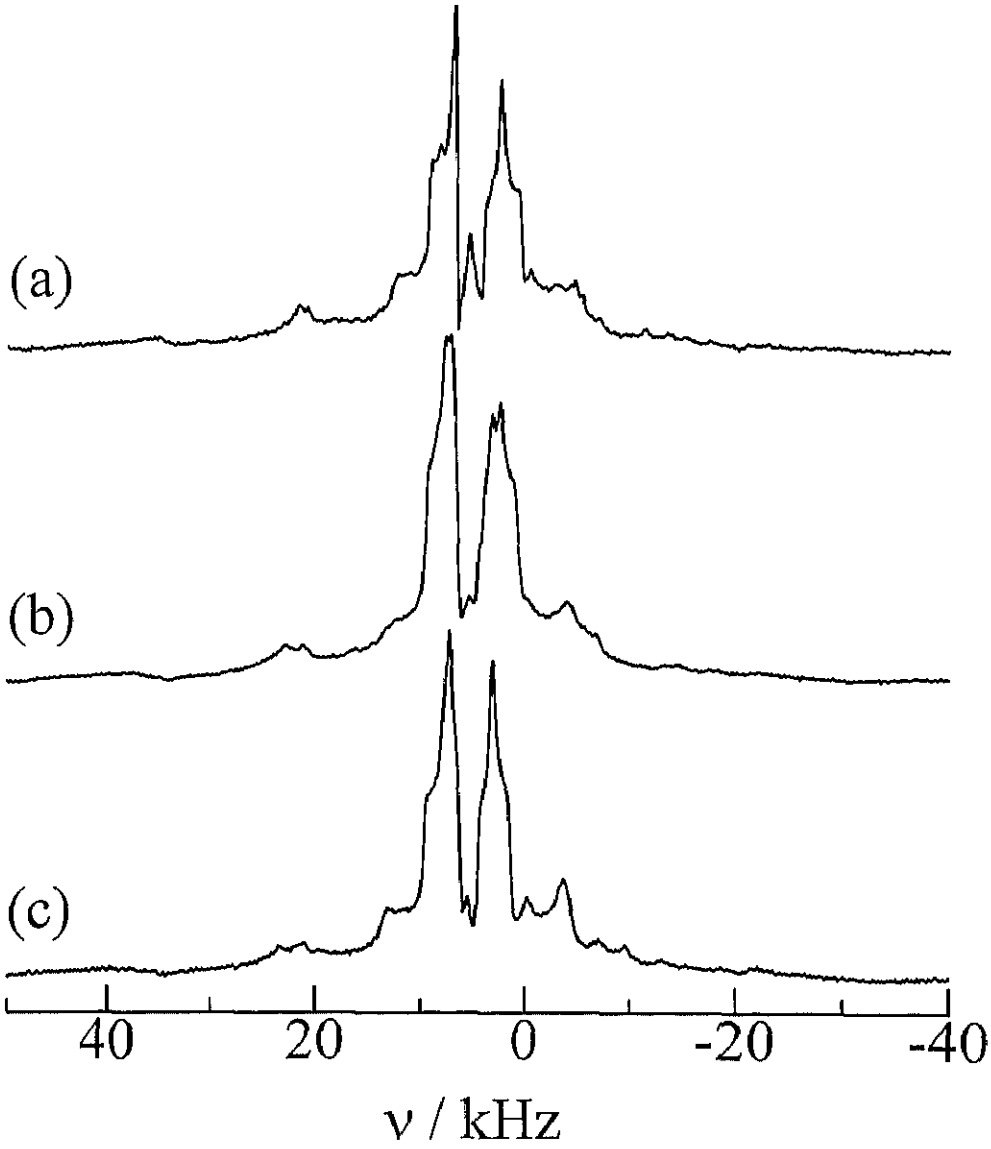

Fig. 2. 23 Quadrupolar perturbed ^{133}Cs NMR spectra measured at 39.4 MHz in the N (a), IC (b) and C phases (c) in the modification-A of Cs_2CdI_4.

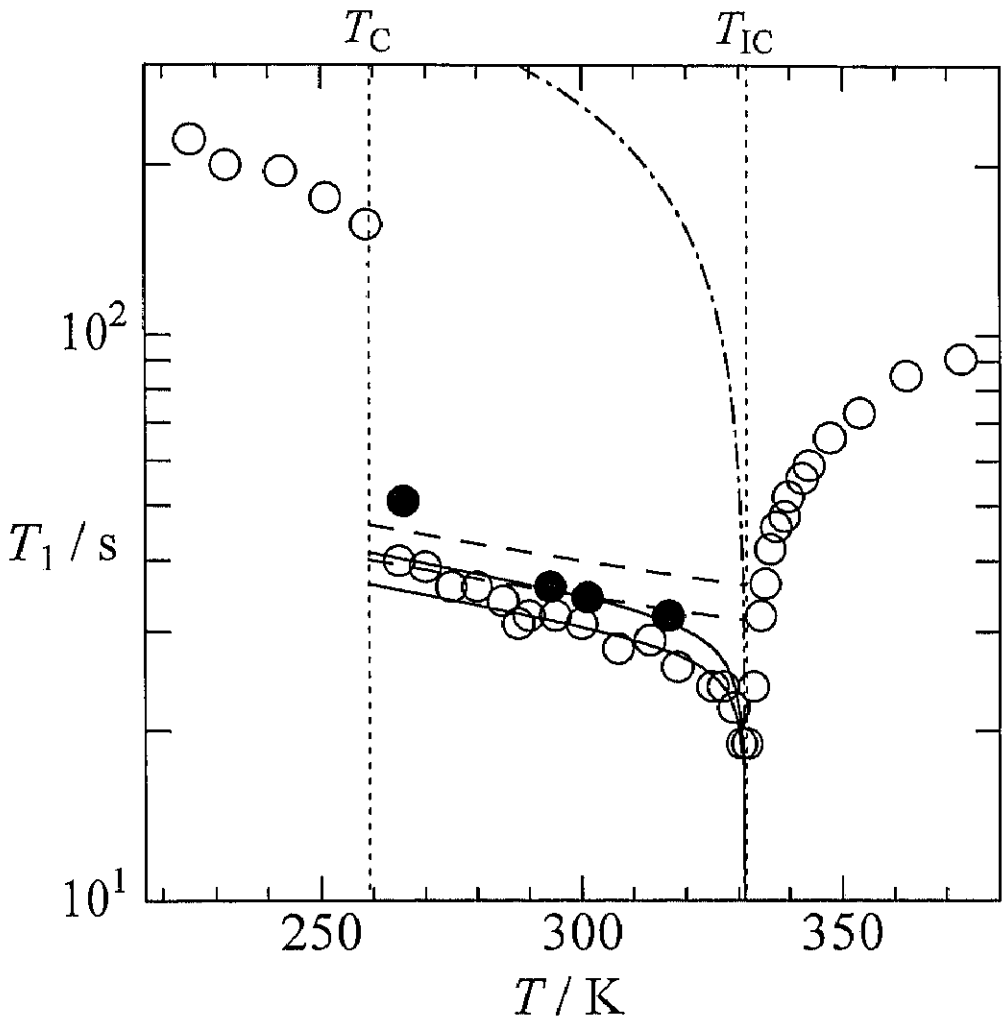

Fig. 2. 24 Temperature and frequency dependences of ^{133}Cs NMR T_1 in the IC phase for the modification-A of Cs_2CdI_4 measured at 39.4 (○) and 52.5 (●) MHZ. Solid lines are the best-fitted curves calculated by introducing phason (broken lines) and amplitudon (chain line) contributions. Vertical doted lines correspond to phase transition temperatures observed by DTA.

2.5.4 Discussion

N phase

The T_1 dip observed in this phase near the phase transition temperature is attributable to the fluctuation of quadrupole interaction caused by the critical slowing down of the lattice vibration due to the second order N-IC phase transition. T_1 can be represented by sum of contributions from two mechanisms. Near the phase transition temperature, however, T_{1l} is considered to become negligible in the total T_1 because T_{1l} values can be estimated to be *ca.* 100 *s* or longer as expected from the observed T_1 at 370 K. So only T_{1c}^{-1} given by eq. (2.12) is taken into account here and the critical exponent ζ can be obtained from the slope of log T_1 vs. log ε plots. The value of ζ in Cs_2CdI_4 was estimated to be 0.62 ± 0.03, which coincides with 0.62 obtained in Cs_2CdBr_4, in the temperature region less than 7 K above the transition temperature (Fig. 2. 25). This value agrees well with the theoretical value of 0.625 calculated for the three-dimensional XY-model which is predicted as the model of driving interaction of the N-IC phase transition [33]. The deviation of calculated T_1 values from the observed one in the temperature region higher than 7 K above the phase transition temperature is attributable to the influence of T_{1l}.

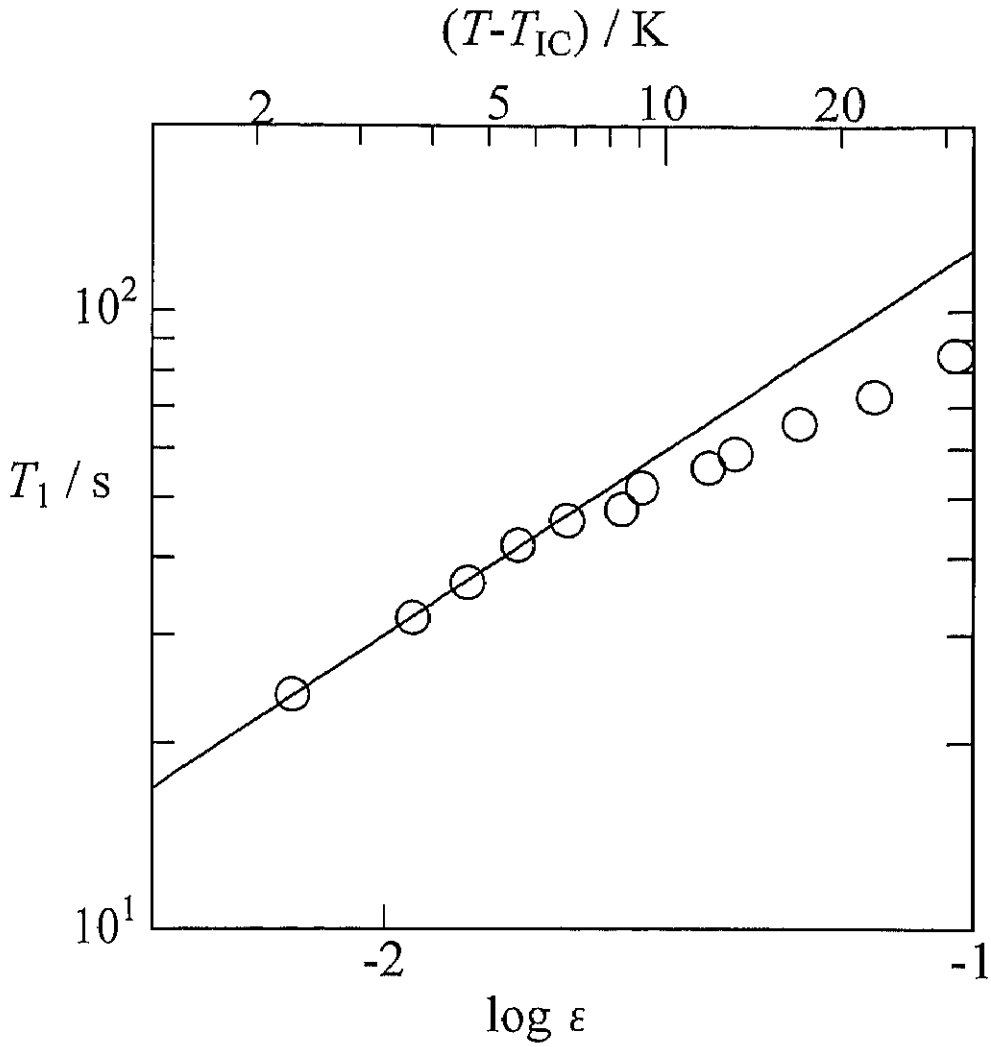

Fig. 2. 25 A critical plot of ^{133}Cs NMR T_1 observed above the N-IC phase transition in the modification-A of Cs_2CdI_4. Solid line is the best-fitted curve using eq. (2.12) in the range of $\varepsilon = (T - T_{IC}) / T_{IC} < -1.7$.

IC Phase

The T_1 values observed in this phase were shorter than those in N and C phases. Upon heating, T_1 sharply decreased near the N-IC transition point. This T_1 behavior is explainable by considering two characteristic lattice modes, amplitudon and phason representing fluctuations of incommensurate modulation [2]. The total T_1 is then expressed as eq. (2.13). Since T_1 values observed in the IC phase are about one order magnitude shorter than those in N and C phases (Fig. 2. 24), the contribution from the normal lattice mode T_{1l}^{-1} is considered to be negligible.

In the plane wave limit, the contributions from amplitudon and phason are given by eq. (2.14) and eq. (2.15), respectively [2, 17]. The frequency dependence of T_1 obtained in the IC phase is represented as $T_1 \propto \omega^{0.45}$. Substituting this frequency dependence of T_1 in eq. (2.15), a small phason gap $\nu_\phi = \omega_\phi / 2\pi$, 0 - 5 MHz, implying to fulfill the condition $\omega_\phi \langle\langle \omega_L$ is observed. Standing on the above discussions, T_1^{-1} observed in the IC phase was fitted by eq. (2.13) - (2.16) i.e., the superposition of contributions from T_{1a}^{-1} and $T_{1\phi}^{-1}$, as shown by solid lines in Fig. 2. 24. Since the contribution from the amplitudon was shown to emerge only in the neighborhood of T_{IC} and could not be separated from the total T_1, the classical value $\zeta' = 0.5$ was assumed of apply eq. (2. 14).

Some deviation of the calculated line from the observed T_1 in the low-temperature region in the IC phase is explainable by the breakdown of the plane wave approximation for the IC modulation. This T_1 behavior resembles to the results obtained in Cs_2CdBr_4 crystals [41] measured in section 2.3.

The splittings of NMR lines observed in this phase (Fig. 2. 23) were caused by

the distribution of the electric field gradient at Cs nuclei due to the IC modulation [2, 20]. The obtained temperature dependences of frequencies at split peaks are shown in Fig. 2. 26. The high frequency branches of both split peaks increased almost linearly with temperature decrease and the others were inappreciably temperature dependent implying that the resonance frequency is governed by the quadratic term in the expanded series in power of the IC modulation amplitude in the non-local case which is taken into account of the phase fluctuation of the modulation wave (section 2.2) [20]. In Cs_2CdI_4, the slow motion regime is acceptable because the relation $\omega_\phi \langle\langle \omega_L$ was obtained from the T_1 analysis described above. But an about twice larger value of critical exponent $\overline{\beta}=1.7\pm0.4$ was estimated from the observed temperature dependences of splitting width in the low-temperature region of the IC phase (Fig. 2. 27). Such an anomalous increase of the critical exponent in this region can be explained by the change of the form in the IC modulation wave, from the plane wave to the multi-soliton, as already reported by ^{87}Rb NMR studies in Rb_2ZnCl_4 and Rb_2ZnBr_4 [22]. This result also suggests that the plane wave limit could not be applied to the low-temperature IC phase below about 290 K in Cs_2CdI_4. This is consistent with the result of above-mentioned T_1 data. .

C phase

In the C phase, ^{133}Cs T_1 is governed by normal lattice vibrations, because the observed T_1 was longer than in IC phase and the high-temperature region in the N phase, and showed a moderate temperature dependence. No anomaly was observed in all temperature region studied in this phase even near the 1st order IC-C transition.

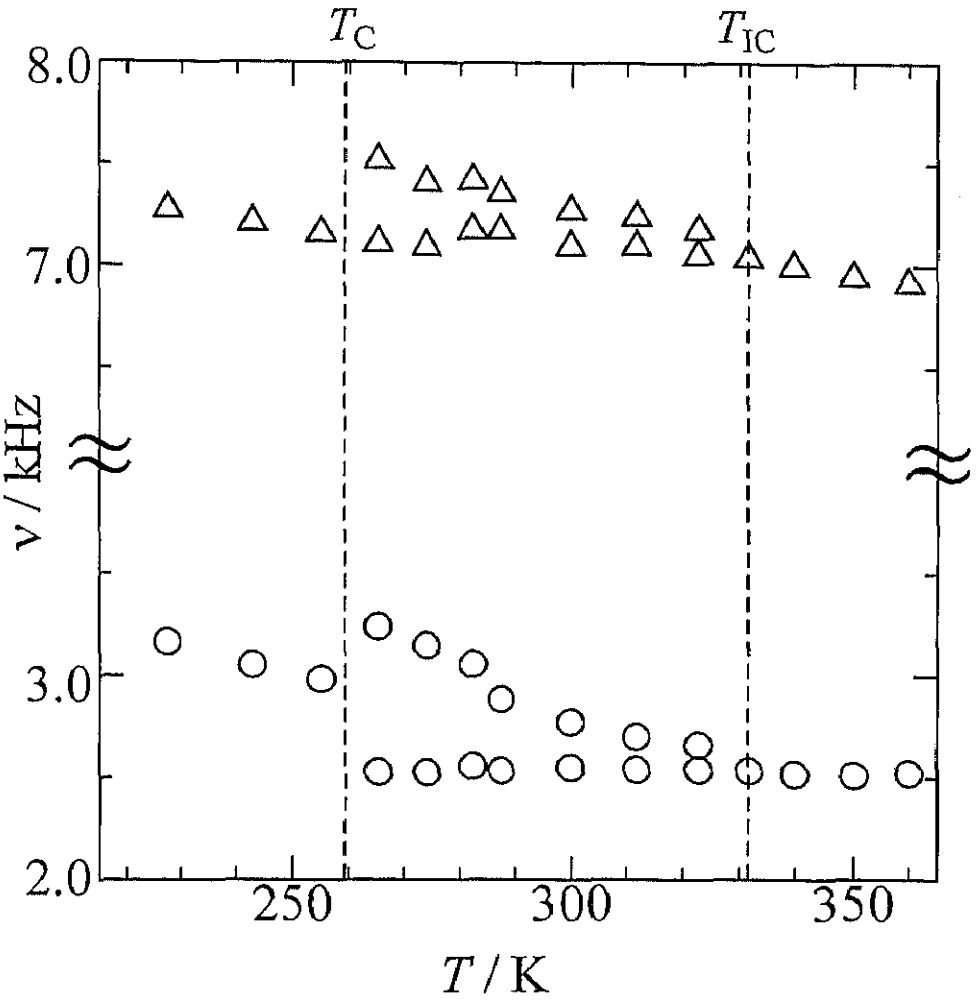

Fig. 2. 26 Temperature dependences of splittings of two central peaks observed in ^{133}Cs NMR spectra for the modification-A of Cs_2CdI_4. Vertical dotted lines correspond to phase transition temperatures observed by DTA.

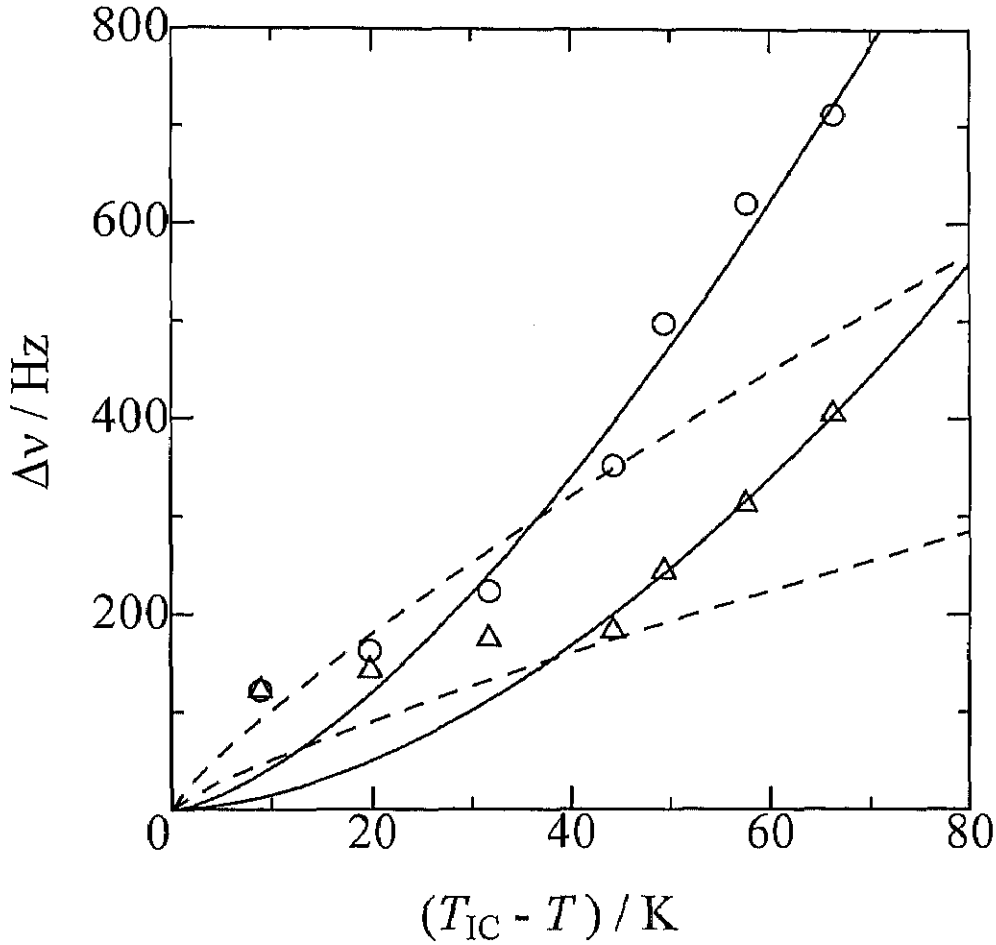

Fig. 2. 27 Temperature dependences of splitting widths $\Delta\nu$ of two central lines in ^{133}Cs NMR spectra for the modification-A of Cs_2CdI_4. Circles and triangle represent $\Delta\nu$ in the low- and high-frequency lines, respectively. Solid and broken lines are best-fit curves using eq. (2.35) with $\bar{\beta}$=1.7 and theoretical value $\bar{\beta}$=0.832, respectively.

2.6 *Cesium tetrachloromercurate Cs_2HgCl_4*

2.6.1 Introduction

Characteristic properties in phase transitions and the IC phase in Cs_2HgCl_4 have been extensively studied by X-ray diffraction [42, 43], birefringence [44, 45], calorimetric [46, 47], dielectric [48-50], spontaneous polarization [49, 50], ^{35}Cl NQR frequency [42, 51, 52], optical [44] and ultrasonic [44, 45, 53, 54] measurements and lattice dynamics simulations [55, 56]. According to the AC calorimetry measurement, Cs_2HgCl_4 undergoes seven phase transitions at T_{IC}=219, T_C=193, T_{C1}=182.5, T_{C2}=177, T_{C3}=173.0, T_{C4}=163.5 and T_{C5}=120 K [47], although the number and temperatures of phase transitions have differently been reported by other methods [44, 46, 50]. A crystallographic study [43] showed that the symmetry of the N phase above T_{IC} is centrosymmetric *Pnma* with displacement disorders in $HgCl_4^{2-}$ complex anions and one of the crystallographically nonequivalent two Cs cations. It was reported that the IC phase obtained between T_{IC} and T_C presumed to transforms into a ferroelectric commensurate (C) phase without centrosymmetry *mm*2 [44], but structures below T_C have not been clarified completely. On the other hand, ^{35}Cl NQR [52], dielectric and Raman scattering [48] measurements revealed different results that the IC phase appears between T_{IC} and T_{C1} [52]. From the optical polarization measurement, the low-temperature phase immediately below T_{C1} is anticipated to be a ferroelastic C phase analogous to those in Cs_2MBr_4 (M=Cd, Hg).

2.6.2 Experimental

Cs_2HgCl_4 crystal was grown by cooling a melted mixture containing stoichiometric amounts of CsBr (purity 99.9%) and $HgCl_2$ (purity 99.9%) purchased from Wako Pure Chemical Industries, Ltd. The obtained crystalline powder was dried *in vacuo* and then sealed in glass sample tubes with nitrogen gas for DTA and NMR measurements.

Differential thermal analysis (DTA) was carried out to confirm reported phase transitions in a range 120-300 K. The sample temperature was determined within ± 0.2 K. X-Ray powder diffraction was measured to confirm lattice parameters and determine those temperature dependences using a Phillips X'Pert PW3050/00 diffractometer in a range 175-360 K.

The ^{133}Cs NMR spectra were measured with a Bruker MSL-300 NMR system at a Larmor frequency of 39.4 MHz in a range 160-361 K. A saturated CsCl aqueous solution was used as a standard of frequency shift and for setting the width of the 90° pulse. All ^{133}Cs NMR spectra obtained from FID signals observed by adding a single detection 90° pulse with the width 4-6 μs. ^{133}Cs NMR T_1 measurements were performed with a Bruker MSL-300 NMR system at a Larmor frequency of 39.4 MHz using the saturation-τ- 90° pulse sequence in the range 160-371 K and also with a Bruker MSL-400 NMR system at 52.5 MHz in 196-215 K to obtain the T_1 frequency dependence. The sample temperature was controlled within ± 0.5 K with a Bruker VT-1000 temperature controller and determined by a copper-constantan thermocouple with the same accuracy. The uncertainty in the T_1 measurement is estimated to be within 5 %.

2.6.3 Results

DTA thermograms measured on heating displayed endothermic anomalies due to phase transitions at 163.0±0.6, 172.2±1.0, 177.3±0.9, 183.1±0.6 and 219.5±0.8 K in good agreement with previously reported phase transition temperatures of T_{C4}, T_{C3}, T_{C2}, T_{C1} and T_{IC} measured by the AC calorimetry [47], respectively. No thermal anomaly corresponding to T_C was not detected around the reported temperature 193 K. In following discussion the IC phase is assumed to form between T_{C1} and T_{IC} as same as the reported NQR study [52].

X-ray powder diffraction patterns obtained at *ca.* 300 K are shown in Fig. 2. 28 together with the pattern simulated using the atomic coordinates reported previously at room temperature [43]. Lattice parameters derived from the experimental pattern observed at *ca.* 300 K together with the reported values shown in parentheses are a = 9.79 Å (9.8136 Å), b = 7.59 Å (7.6018 Å) and c = 13.42 Å (13.4201 Å). Temperature dependences of lattice parameters are shown in Fig. 2. 29. All lattice parameters and $V^{1/3}$ decreased upon cooling and showed dips around T_{C3}. It is noted that b, c and $V^{1/3}$ displayed critical contractions in the neighborhood of T_{IC}.

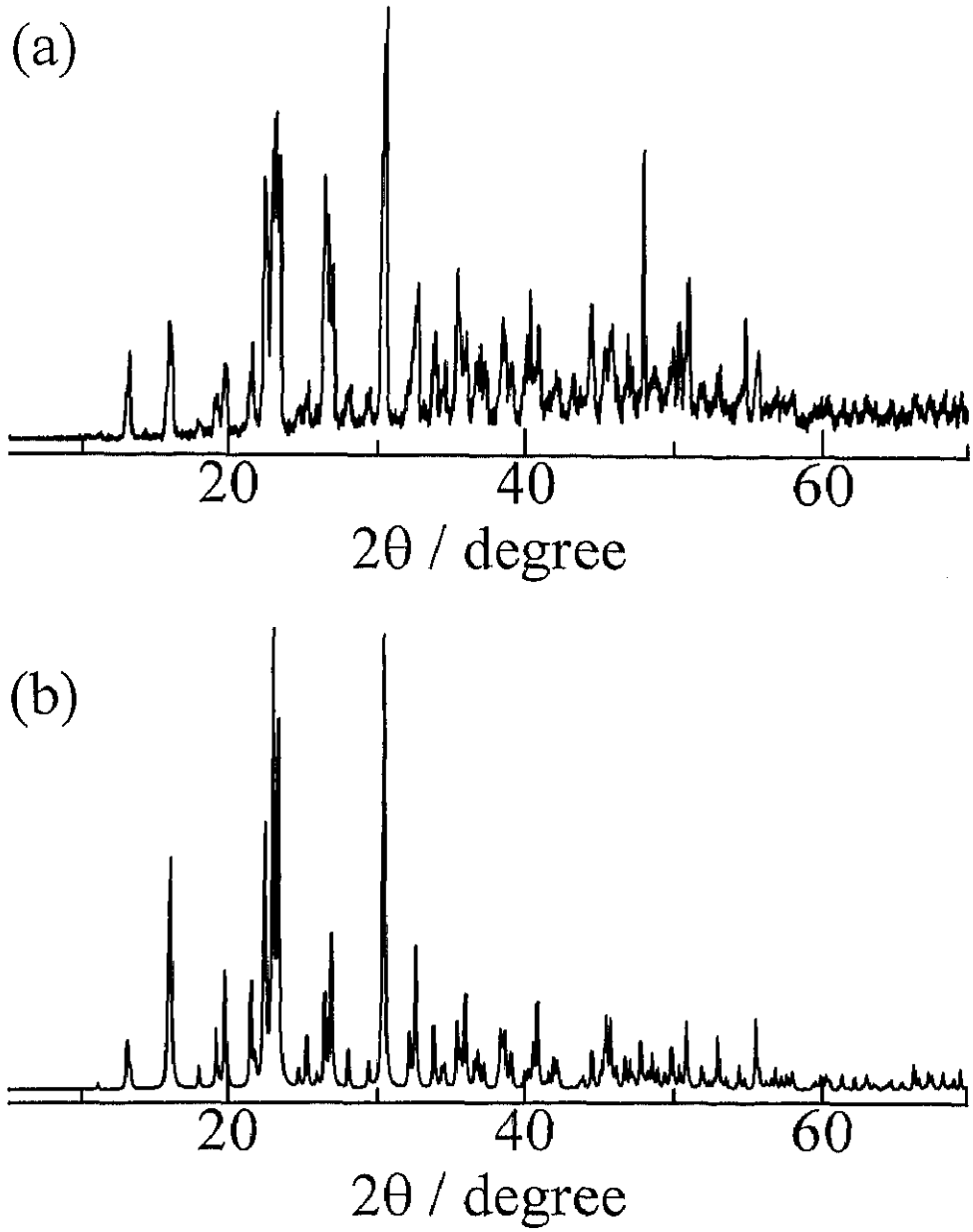

Fig. 2. 28 (a) An X-ray powder diffraction pattern observed at ca. 300 K in Cs_2HgCl_4. (b) A simulated powder pattern using reported atomic coordinates [43].

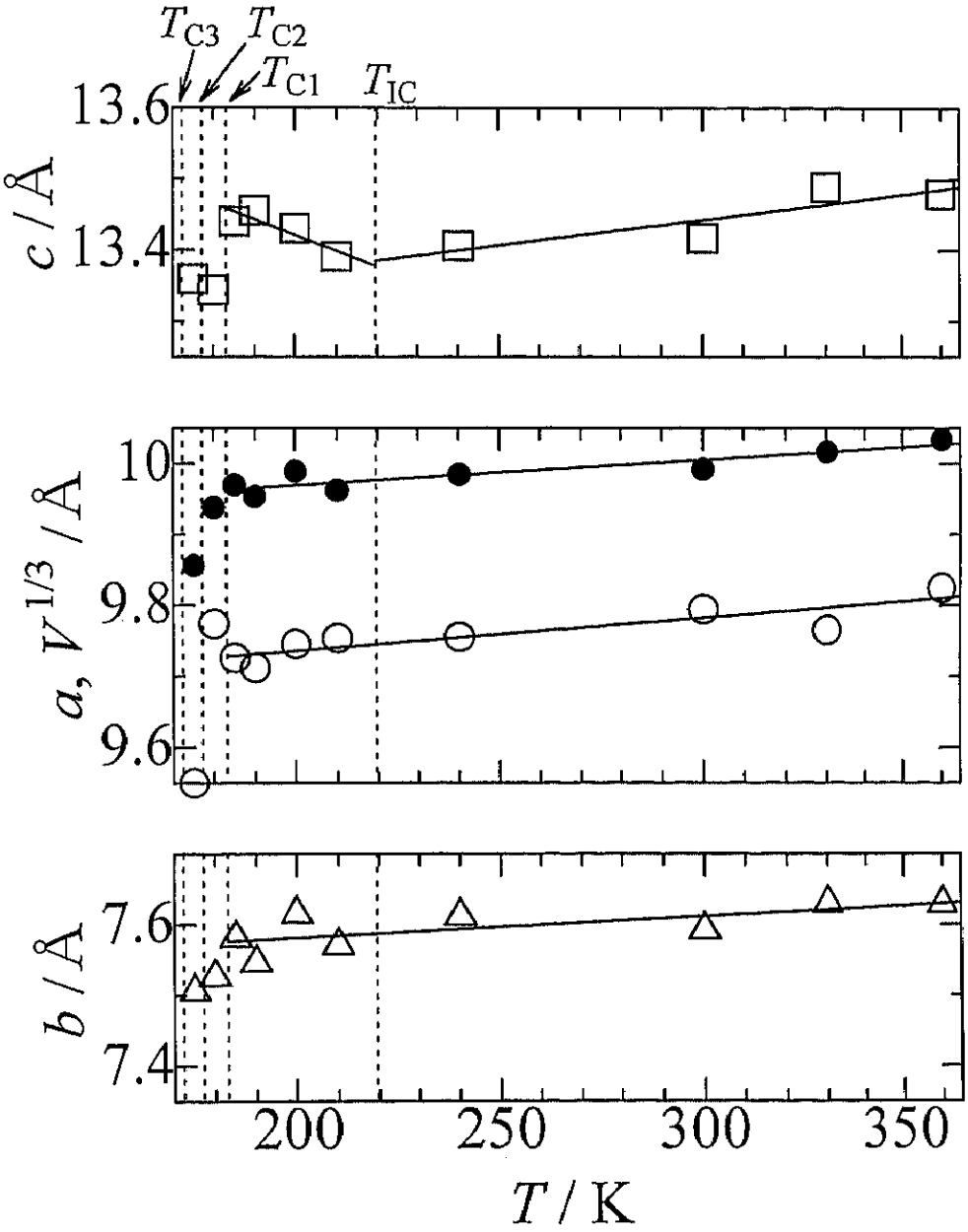

Fig. 2. 29 Temperature dependences of lattice parameters a (○), b (△) and c (□), and the cube root of a unit cell volume $V^{1/3}$ (●) in Cs_2HgCl_4.

The quadrupolar perturbed ^{133}Cs NMR spectra observed in the N, IC and lowest temperature phases are shown in Fig. 2. 30. The observed line-shapes are explained by the superposition of two 1st order perturbed spectra. This result is consistent with the reported crystal structure containing two crystallographically nonequivalent Cs ions [43]. The estimation of quadrupole coupling constants e^2Qq/h and non-zero asymmetric parameters η are determined to be 150±30 kHz and 0.1±0.1, and 230±80 kHz and 0.5±0.2, respectively, in the N phase by referring to the values obtained from ^{133}Cs NMR measurement in an analogous single crystal compound Cs_2HgBr_4 [32]. In the low-temperature range of the IC phase, the two central peaks showed small splittings typical of the IC modulation.

Temperature and frequency dependences of ^{133}Cs NMR T_1 are shown in Fig. 2. 31. The T_1 showed a discontinuous jump at T_{C1} reported to be a 1st order phase transition temperature. T_1 decrease was observed around T_{IC} and T_{C3}. These transitions have been reported to be a 2nd [46, 48] and a 1st order one [50], respectively. No remarkable T_1 anomaly was observed at T_{C2} and T_{C4}. T_1 values observed between T_{IC} and T_{C1} were shorter than those in the C phase and the high temperature region of the N phase, and showed frequency dependency. Such short and frequency dependent T_1 values are characteristic of the IC phase [2]. A slight decrease of T_1 within the experimental error was observed at 193 K. This might correspond to the reported transition to the commensurate phase although the change is remarkable at the IC-C transition in most cases [2].

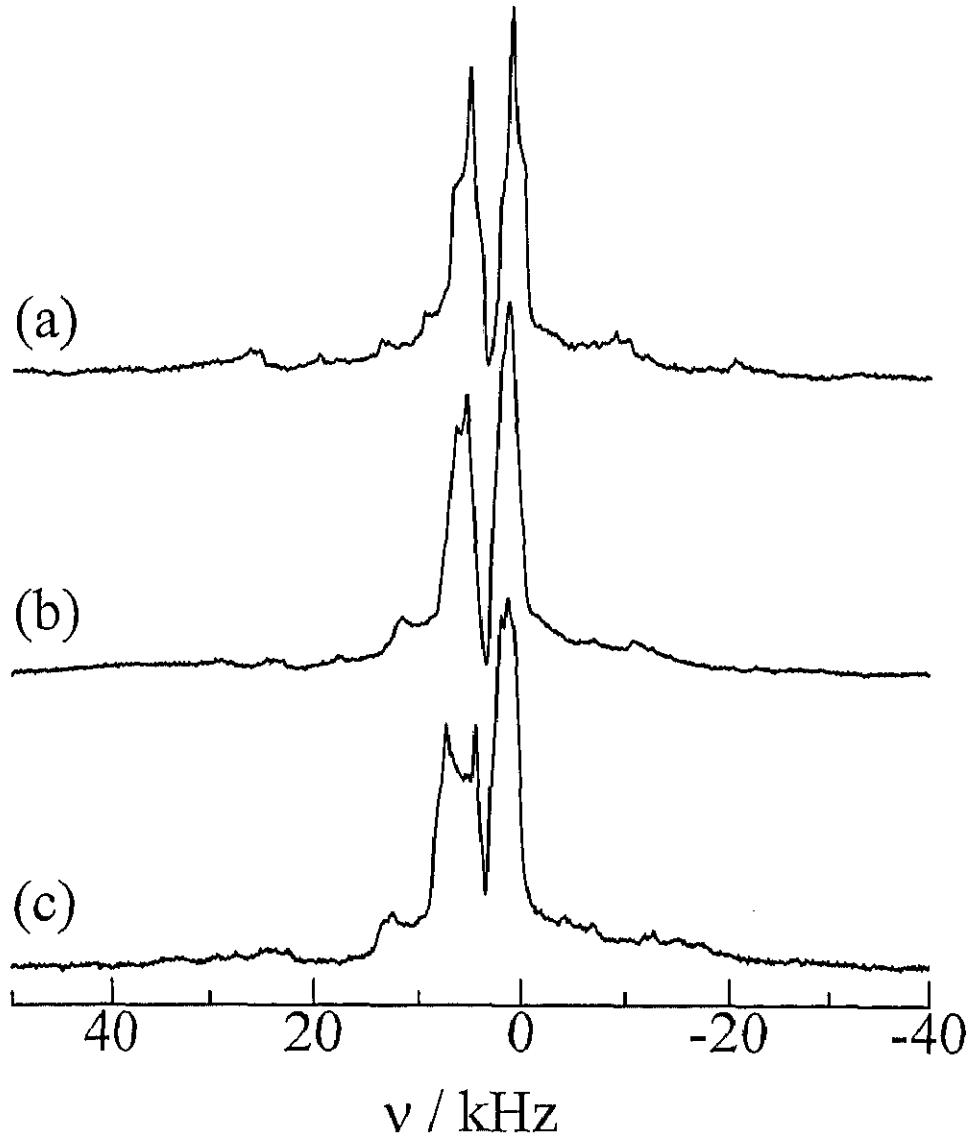

Fig. 2. 30 Quadrupolar perturbed ^{133}Cs NMR spectra measured at 39.4 MHz in the N (a), IC (b) and lowest temperature phases (c) in Cs_2HgCl_4.

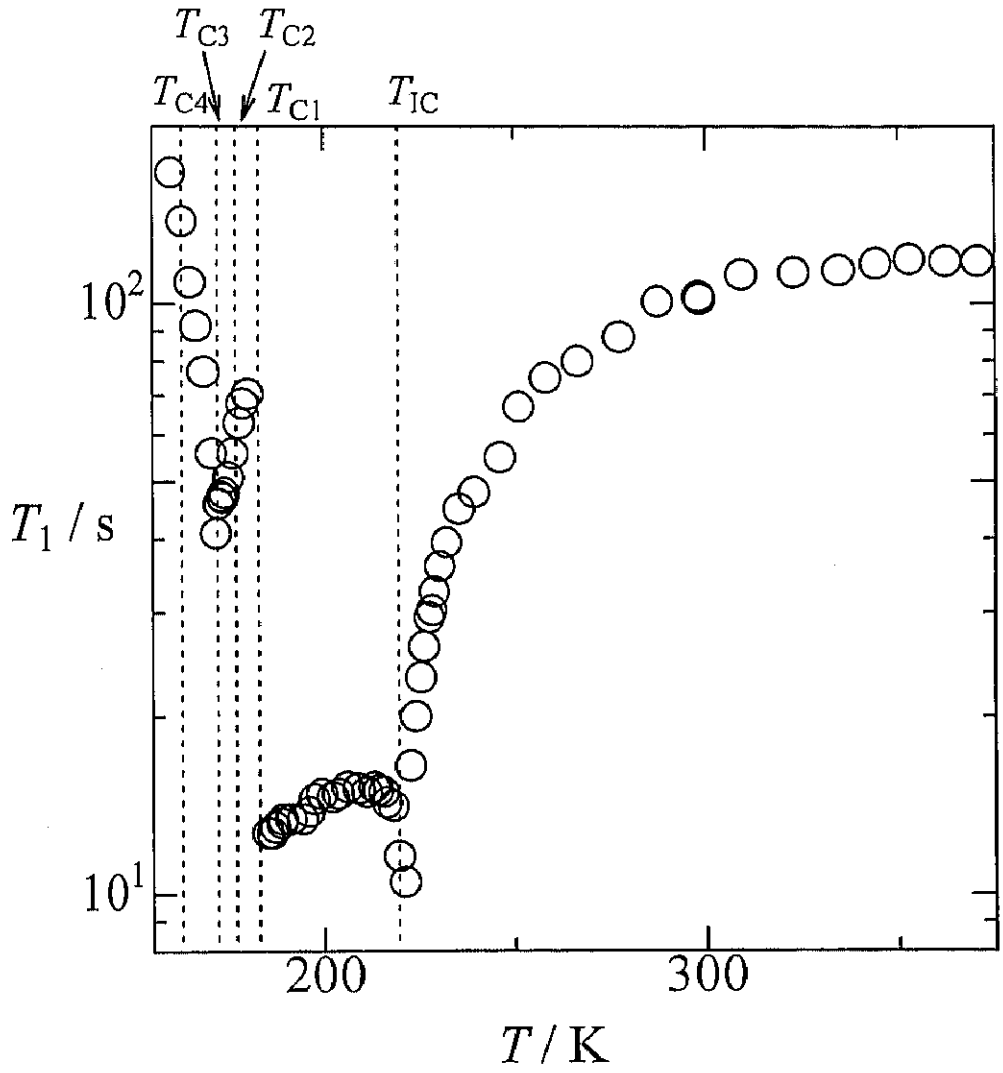

Fig. 2. 31 A temperature dependence of ^{133}Cs NMR T_1 measured at 39.4 MHz in Cs_2HgCl_4. Doted lines correspond to phase transition temperatures observed by DTA.

2.6.4 Discussion

N phase

The ^{133}Cs NMR T_1 dip observed in the vicinity of T_{IC} can be explained by the critical fluctuation of the quadrupolar interaction due to the 2nd order phase transition. T_1 in the N phase can be represented by the sum of contributions from normal lattice vibrations (T_{1l}^{-1}) and the critical fluctuation (T_{1c}^{-1}). Near the phase transition temperature, T_{1l} became negligible in the total T_1. Thus, only T_{1c}^{-1} given by eq. (2.12) may be taken into account in this temperature region. The critical exponent ζ can be obtained from the log T_1 vs. log ε plots in the vicinity of the transition point. Actually, log T_1 vs. log ε plots gave an almost straight line in a range less than 10 K above the transition temperature T_{IC} as shown in Fig. 2.32.

The critical exponent ζ was determined to be 0.615 ± 0.025. This value agrees well with the value 0.62 ± 0.02 obtained in Cs_2CdBr_4 [41] and of $\zeta = 0.625$ calculated for the three-dimensional *XY* model [8, 9, 13]. The theoretical treatment has predicted that the three-dimensional *XY* model is acceptable for the transition from normal to the IC phase with one-dimensional modulation because the order parameter has two components, i.e., the amplitude and the phase of the incommensurate modulation.[23] The present result in Cs_2HgCl_4 is different from that in Cs_2HgBr_4 [41], where T_1 behavior could be explained by the classical mean field approximation due to the long-range interionic interaction.

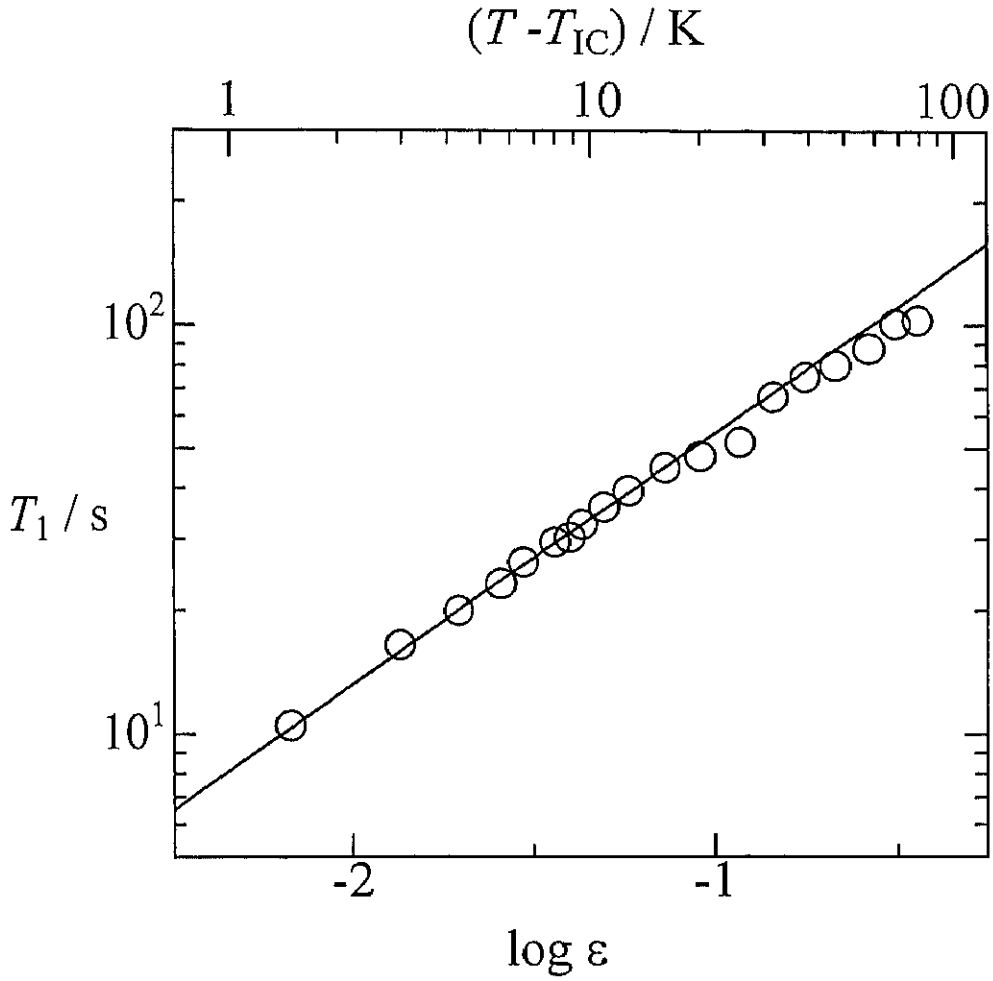

Fig. 2. 32 A critical plot of ^{133}Cs NMR T_1 above the N-IC phase transition in Cs_2HgCl_4. Solid line is the best-fitted curve using eq. (2.12) in the range of $\varepsilon = (T - T_{IC}) / T_{IC} < -1.4$.

IC phase

It is noted that the short T_1 was observed in the IC phase compared with those in N and C phases. The frequency dependence of T_1 values obtained in the IC phase between 190 K and 210 K can be expressed by a relation, $T_1 \propto \omega_L^{0.45}$ (Fig. 2. 33). Since the phason gap $\nu_\phi = \omega_\phi / 2\pi$ can be estimated to be 0 - 5 MHz from eq. (2.15) by assuming above frequency dependence of T_1 in the plane wave limit, the phason gap is considered to fulfill the condition $\omega_\phi \langle\langle \omega_L$. In Cs_2HgCl_4, T_1 observed in the IC phase could not be fitted by the same eqs. (2.13)-(2.16) used a in the analysis Cs_2CdBr_4, Cs_2HgBr_4 and Cs_2CdI_4. The fact that the observed T_1 decreased upon cooling in the low-temperature region of the IC phase is the opposite behavior to that of the plane wave limit. This suggests that the multi-soliton model is more suitable than the plane wave model in this temperature region as predicted by Levanyuk taking into account of the thermodynamic potential [57].

The observed T_1 values in this phase are fitted (solid lines in Fig. 2. 33) by using eqs. (2.10)-(2.16), (2.19), (2.26) and (2.27) assuming ζ'=0.5 for the contribution from amplitudon (chain line) and also assuming the plane wave limit above *ca.* 210 K (bold broken lines) and the multi-soliton limit below this temperature (fine broken lines) for phason. From the fitting, $T_{C'} \approx 172$ K as the phason softening temperature is derived, although the IC phase transforms into the C phase before reaching this temperature. Furthermore, the changing from the relaxatory phason to the damping oscillation phason in the IC phase of Cs_2HgCl_4, which was not observed in corresponding phases of Cs_2CdBr_4 and Cs_2HgBr_4 [41], implies the occurrence of crossover from order-disorder to displacive behavior, which seems to be connected with the small size of the complex

anion. Such a crossover was also reported by Raman scattering measurements in Rb_2ZnCl_4 and Rb_2ZnBr_4 [58].

Temperature dependences of frequencies of two central peaks in the N, IC and C phases are shown in Fig. 2. 30. Splittings in the IC phase were observed in the high-frequency central peaks below about 190K. The splitting widths ($\Delta\nu$) are roughly estimated from the spectra. This splitting is expected to be related with the amplitude of the IC modulation. The obtained temperature dependences of the frequencies at split peaks are shown in Fig. 2. 34. They show different behavior that ones are inappreciably temperature dependent and the others increase almost linearly with temperature decrease. These results imply that the resonance frequency is governed by the quadratic term in the expanded series in power of the IC modulation amplitude as discussed in subsection 2.2.2. The critical exponent $\bar{\beta}$ in eq. (2.35) estimated to be 1.8 ± 0.4 is too large compared with $\bar{\beta}$=0.832 [22] derived theoretically for the *XY* model (Fig. 2. 35). This anomalous $\bar{\beta}$ value is explainable as follows: Reliable values of $\Delta\nu$ could be obtained only in low-temperature region of the IC phase where the IC modulation wave is not characterized by the plane wave but the multi-soliton limit as mentioned above.

C phases

In this phase, we can anticipate that the modulation can no more slide freely and the phason becomes a normal lattice mode resulting in long T_1 as shown in Fig. 2. 31. The T_1 dip observed around T_{C3}=172.2 K is attributable to the contribution from the phase transition.

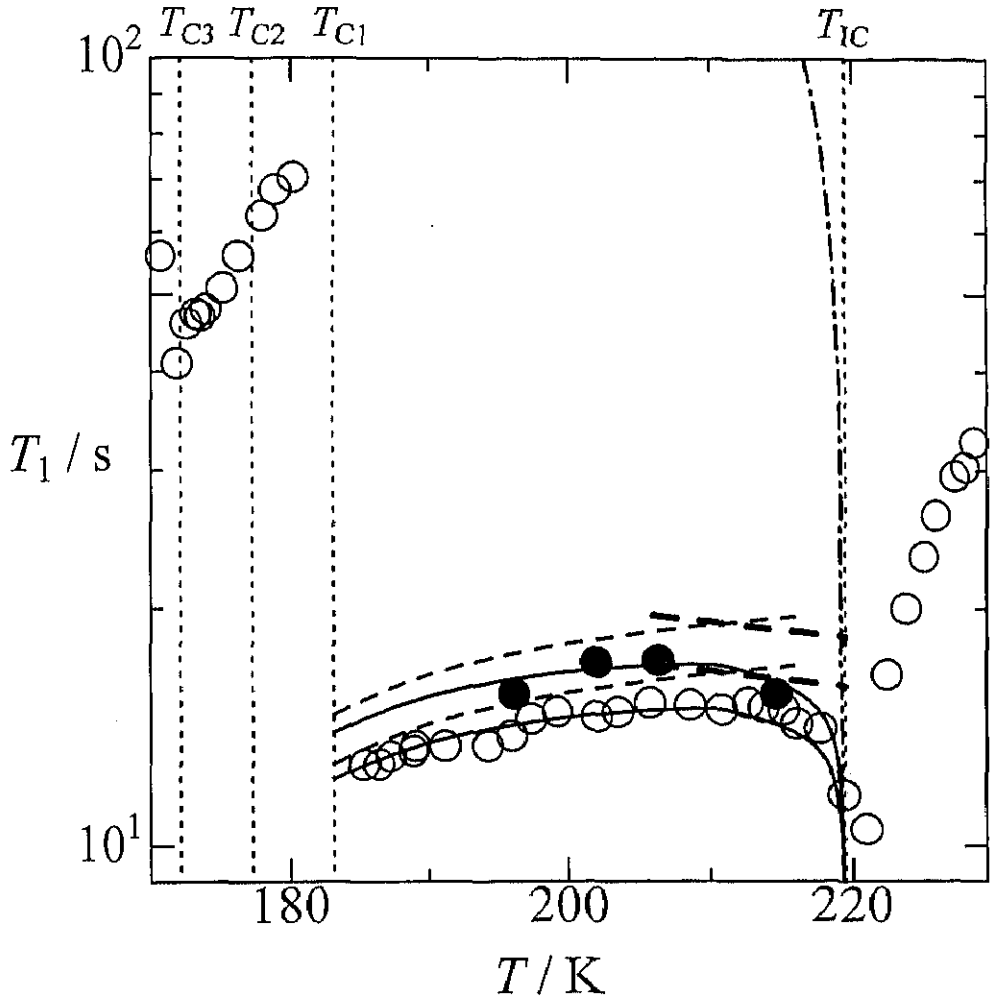

Fig. 2. 33 Temperature and frequency dependences of ^{133}Cs NMR T_1 in the IC phase of Cs_2HgBr_4 measured at 39.4 (○) and 52.5 (●) MHZ. Solid lines are the best-fitted curves calculated by introducing phason (broken lines) and amplitudon (chain line) contributions. Vertical doted lines correspond to phase transition temperatures observed by DTA.

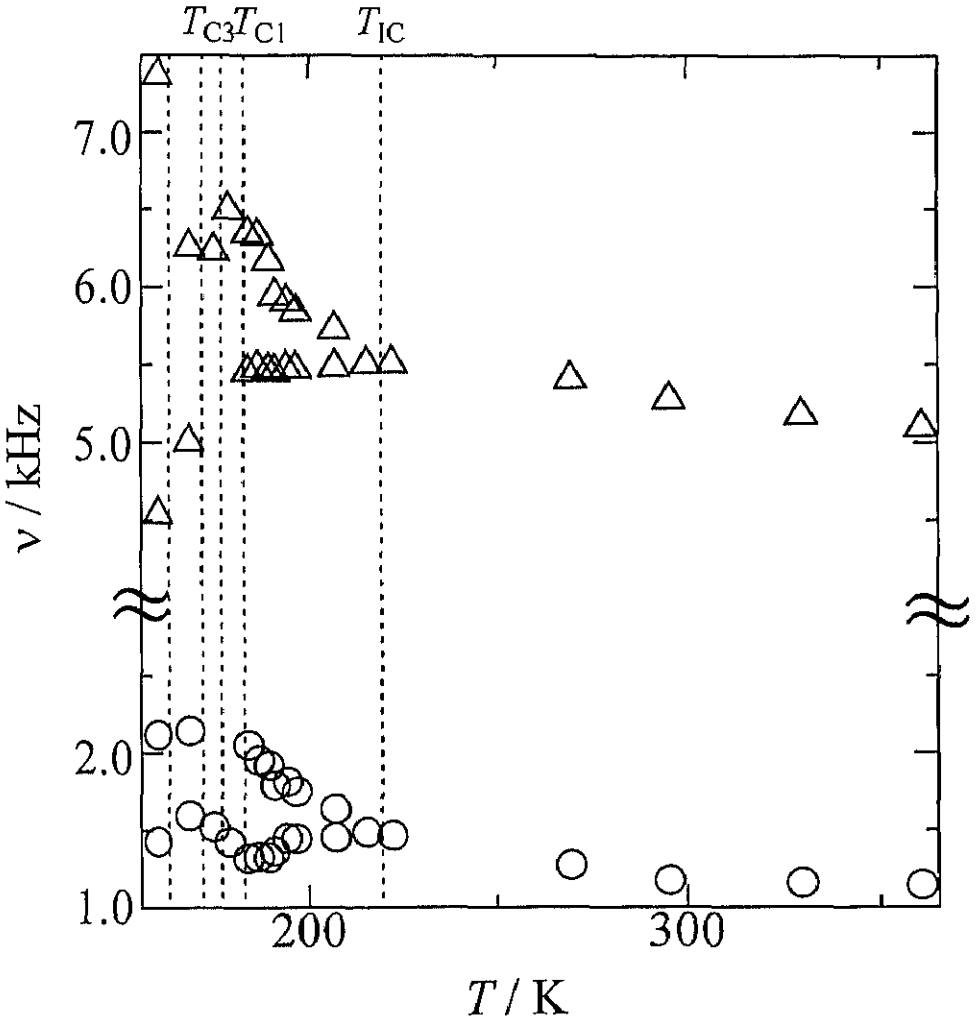

Fig. 2. 34 Temperature dependences of splittings of two central peaks observed in ^{133}Cs NMR spectra for Cs_2HgCl_4. Vertical dotted lines correspond to phase transition temperatures observed by DTA.

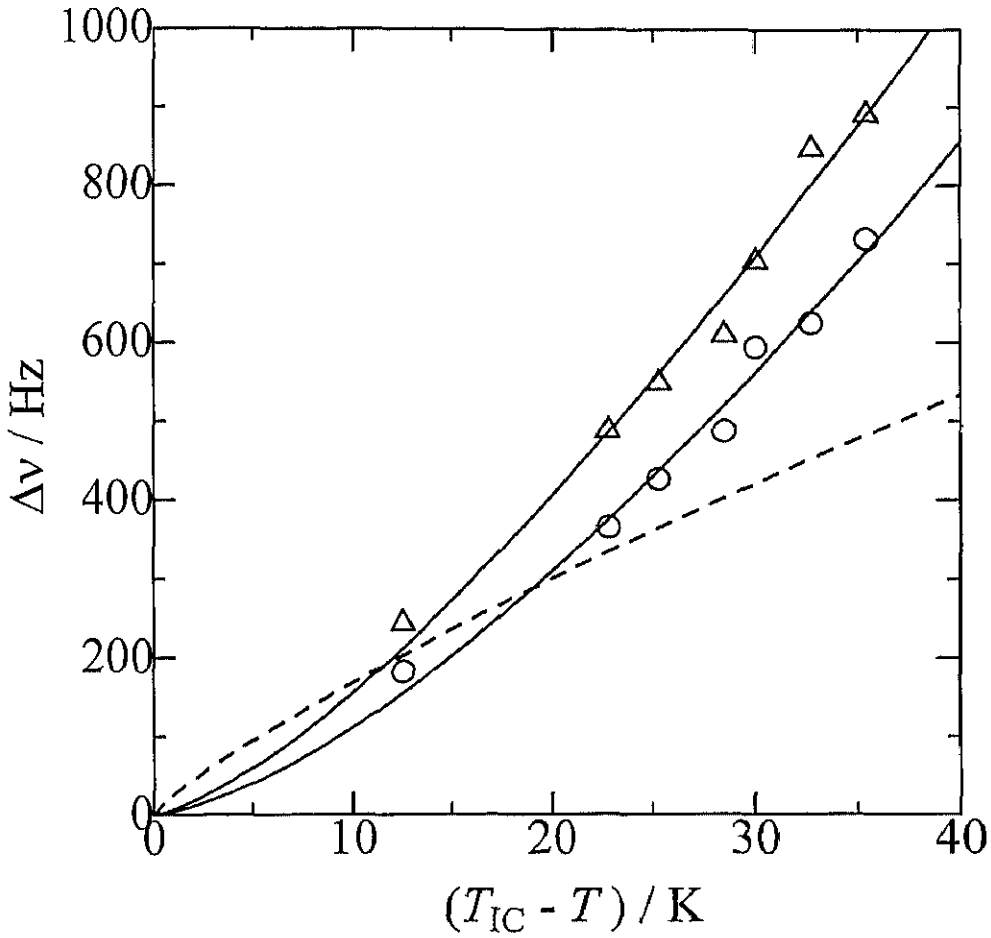

Fig. 2. 35 Temperature dependences of splitting widths $\Delta\nu$ of two central lines in ^{133}Cs NMR spectra for Cs_2HgCl_4. Circles and triangle represent $\Delta\nu$ in the low- and high-frequency lines, respectively. Solid and broken lines are best-fit curves using eq. (2.35) with $\bar{\beta}$=1.8 and theoretical value $\bar{\beta}$=0.832, respectively.

2.7 *Interionic interaction and transition mechanism*

In the above discussions, the difference and analogy of the critical behavior at the N-IC phase transition and the temperature variation of the IC modulation wave in the IC phase in some Cs_2MX_4 compounds were clarified. In this section, the behavior of the lattice dynamics is tried to explained by means of the interionic interaction between Cs^+ cations and complex anions. This attempt seems to be reasonable because the results of the critical exponent in Cs_2CdBr_4 agrees well with those of Cs_2CdI_4 and Cs_2HgCl_4 but differs from that in Cs_2HgBr_4, although Cs_2HgBr_4 and Cs_2CdBr_4 have the analogous anionic size [30, 59] and the lattice volume [31]. The halogen ionicity can be estimated from e^2Qq/h using the Townes-Dailey relation [60]:

$$e^2Qq/h = (1-s)(1-i)(e^2Qq/h)_{atom}, \tag{2.20}$$

where s is the contribution from s electrons in the chemical bond and assumed to be 0.15, i is the ionic character of the M-X bonds, i.e., (1 - i) affords the covalency, and $(e^2Qq/h)_{atom}$ is the e^2Qq/h of atomic halogen. The averaged ionicities i. e., negative charges, of halogen in the complex anion are calculated by eq. (2.20) to be 0.699 for $HgBr_4^{2-}$, 0.783 for $CdBr_4^{2-}$, 0.741 for CdI_4^{2-} and 0.733 for $HgCl_4^{2-}$ from reported NQR frequencies[23, 52, 61] observed near room temperature by assuming η=0. We can see that $CdBr_4^{2-}$, CdI_4^{2-} and $HgCl_4^{2-}$ have more ionic halogens than $HgBr_4^{2-}$. This difference in the halogen ionicity seems to induce the different behavior, i.e., the non-classical three-dimensional *XY* behavior near the N-IC phase transition in Cs_2CdBr_4, Cs_2CdI_4 and Cs_2HgCl_4 crystals, whereas the classical mean field behavior in Cs_2HgBr_4

due to the long-rang interionic interaction.

2.8 Conclusion

^{133}Cs NMR T_1 observed in Cs_2CdBr_4, Cs_2CdI_4, Cs_2HgCl_4 and Cs_2HgBr_4 showed sharp dips in the vicinity of N-IC transitions. From the analysis of the critical exponents in N phases, the phase transitions behavior of the former three compounds are described by the three-dimensional *XY* model while the last one by the classical mean field approximation. Since many compounds with the IC phase transition have been reported to show the non-classical behavior, the result in this compound can be considered to be exceptional.

In IC phases of Cs_2CdBr_4 and Cs_2CdI_4, the T_1 could be reproduced by the sum of contributions from the phason with small gaps, 0 - 2 and 0 - 5 MHz, respectively, and amplitudon in the plane wave limit. This model is, however, inapplicable in the vicinity of the IC-C transition where the temperature dependence of T_1 can be explained by the model of the multi-soliton limit rather than the plane wave. In Cs_2HgBr_4, the observed T_1 in the whole IC phase could be explained by the plane wave limit with the sum of contributions from the phason with a small gap, 0 - 8 MHz, and amplitudon in the plane wave limit. In Cs_2HgCl_4, the T_1 in the IC phase can be also reproduced by the sum of contributions from the phason with a small gap, 0 - 5 MHz, and amplitudon. In the low-temperature range of the IC phase, however, the temperature dependence of T_1 can be explained by the IC phase modulation of the damping oscillator multi-soliton model rather than the relaxator mode. This change from the relaxatory phason to the damping oscillation phason in the IC phase of Cs_2HgCl_4 implies the crossover between order-

disorder and displacive behavior which seems to be connected the small size of the complex anion.

In the low-temperature region of the IC phase in Cs_2CdI_4 and Cs_2HgCl_4, splittings of central peaks of ^{133}Cs NMR spectra could be detected and the splitting width ($\Delta\nu$) increases with the temperature decrease.

References in Chapter 2

[1] H. Z. Cummins, *Phys. Rep.*, **185** (1990) 211 and references therein.

[2] R. Blinc, *Phys. Rep.*, 79 (1981) 331.

[3] A. Abragam, *The Principles of Nuclear Magnetism*, Oxford University Press, Oxford, 1961, Chap. 9.

[4] A. Rigamonti, *Adv. Phys.* **33** (1984) 115.

[5] K. Yoshida and T. Moriya, *J. Phys. Soc. Jpn.*, **11** (1956) 33.

[6] A. R. West, *Basic Solid State Chemistry*, John Wiley & Sons Ltd., 1988, Chap. 2.

[7] G. Bonera, F. Borsa and A. Rigamonti, *Phys. Rev.* **B 2** (1970) 2784.

[8] K.-P. Holzer, J. Petersson, D. Schüßler, R. Walish, U. Hächer and D. Michel, *Europhys. Lett.*, **31** (1995) 213.

[9] K.-P. Holzer, J. Petersson, D. Schüssler, R. Walish, U. Hächer and D. Michel, *Phys. Rev. Lett.*, **71** (1993) 89.

[10] W. Gebhardt and U. Krey, *Phasenübergänge und Kritische Phänomene*, Friedr. Vieweg & Sohn, Braunschweig, 1980, Chap. 1.

[11] H. E. Stanley, *Introduction to Phase Transitions and Critical Phenomena*, Clarendon Press, Oxford, 1971, Chap. 3.

[12] W. Gebhardt and U. Krey, *Phasenübergänge und Kritische Phänomene*, Friedr. Vieweg & Sohn, Braunschweig, 1980, Chap. 3.

[13] C. Babnuls and C. Bervillier, *Phys. Rev.* **B 32** (1985) 7209.

[14] W. A. Overhauser, *Phys. Rev.* **B 3** (1971) 3173.

[15] W. L. McMillan, *Phys. Rev.* **B 14** (1976) 1496.

[16] W. L. McMillan, *Phys. Rev.* **B 16** (1977) 4655.

[17] P. Mischo, F. Decker, U. Häcker, K.-P. Holzer and J. Petersson, *Rhys. Rev. Lett.*, **78** (1997) 2152.

[18] C. P. Slichter, *Principles of Magnetic Resonance*, 3rd ed., Springer-Verlag, New York, 1990, Chap. 10.

[19] M. H. Cohen and F. Reif, *Solid State Phys.*, **5** (1957) 321.

[20] R. Blinc, P. Prelovšek, V. Rutar, J. Seliger and S. Žumer, *Incommensurate Phases in Dielectrics 1. Fundamentals*, ed. R. Blinc and A. P. Levanyuk, North

Holland, Amsterdam, 1986, Chap. 4.

[21] F. Borsa and A. Rigamonti, *Structural Phase Transitions II*, ed. K. A. Müller and H. Thomas, Splinger-Verlag, New York, 1991, Chap. 2.

[22] R. Walisch, J. M. Perez-Mato and J. Petersson, *Rhys. Rev.* **B 40** (1989) 10747.

[23] S. Plesko, P. Kind and H. Arend, *Phys. Stat. Sol. A*, **61** (1980) 87.

[24] H. Nakayama, N. Nakamura and H. Chihara, *J. Phys. Soc. Jpn.* **56** (1987) 2927.

[25] N. L. Speziali and G. Chapuis, *Acta Crystallogr. B*, **45** (1989) 20.

[26] S. Plesko, R. Kind and H. Arend, *Ferroelectrics*, **26** (1980) 703.

[27] V. Rodriguez, M. Couuzi, A. Gomez-Cuevas and J. P. Chaminade, *Phase Transit.* **31** (1991) 911.

[28] P. Kužel, P. Moch, A. Gomez-Cuevas and V. Dvořák, *Phys. Rev.* **B 49** (1994) 6553.

[29] P. Kužel, V. Dvořák and P. Moch, *Phys. Rev.* **B 49** (1994) 6563.

[30] D.Altermatt, H.Arend, A.Niggli and W.Petter, *Mat. Res. Bull.*, **14**(1979) 1391.

[31] D. Altermatt, H. Arend, V. Gramlich, A. Niggli and W. Petter, Acta Crystallogr. *B*, **40** (1984) 347.

[32] A. A. Boguslavskii, Yu. N. Ivanov, A. I. Krieger, A. K. Moskalev, V.I. Pakhomov and R. Sh. Lotfullin, *Phys. Stat. Sol. B.* **161** (1990) K49.

[33] R. A. Cowley and A. D. Bruce, *J. Phys. C: Solid State Phys.*, **11** (1978) 3577.

[34] S. Plesko, V. Dvořák, R. Kind and A. Treindl, *Ferroelectrics*, **36** (1981) 331.

[35] V. P. Dmitriev, Yu. I. Yuzyuk, Yu. I. Durnev, L. M. Rabkin, E. S. Larin and V. I. Pakhomov, *Sov. Phys. Solid State*, **31** (1989) 770.

[36] C. B. Pinheiro, A. Jório, M. A. Pimenta and N. L. Speziali, *Acta Crystallogr.*, **B 54** (1998) 197.

[37] A. Jório, M. S. S. Dantas, C. B. Pinheiro, N. L. Speziali and M. A. Pimenta, *Phys. Rev.* **B 57** (1998) 203.

[38] K. S. Aleksandrov, I. N. Flerov, I. T. Kokov, A. I. Kruglik, S. V. Melnikova and E. V. Shemetov, *Ferroelectrics*, **79**, 137 (1988).

[39] K. S. Aleksandrov, S. V. Melnikova, I. N. Flerov, A. D. Vasilev, A. I. Kruglik and I. T. Kokov, *Phys. Stat. Sol. A*, **105**, 441 (1988).

[40] V. Touchard, M. Louër, J. P. Auffredic and D. Louër, *Rev. Chim. Min.*, **24**, 414

(1987).

[41] K. Suzuki, S. Ishimaru and R. Ikeda, *J. Phys. Soc. Jpn.*, **68** (1999) 1963.

[42] V. I. Pakhomov, A. V. Goryunov, I. N. Ivanova-Korfini, A. A. Boguslavskii and R. Sh. Lotfullin, *Russ. J. Inorg. Chem.*, **37** (1992) 259.

[43] B. Bagautdinov, J. Luedecke, M. Schneider and S. V. Smaalen, *Acta Crystallogr. B*, **54** (1998) 626.

[44] O. G. Vlokh, V. G. Gribik, A. V. Kityk, O. M. Mokryi, I. D. Olekseyuk and S. A. Piroga, *Sov. Phys. Crystallogr.*, **35** (1990) 873.

[45] A. V. Kityk, V. P. Soprunyuk, O. G. Vlokh, I. D. Olekseyuk and S. A. Piroga, *Sov. Phys. Solid State*, **34** (1992) 1091.

[46] V. V. Petrov, A. Yu. Khalakhan, V. G. Pitsyuga and V. E. Yachmenev, *Sov. Phys. Solid State*, **30** (1988) 906.

[47] S. N. Kallaev, A. M. Aliev, Sh. B. Abdulvagidov and A. B. Batdalov, *Phys. Solid State*, **39** (1997) 153.

[48] V. P. Dmitriev, Yu. I. Yuzyuk, A. V. Tregubchenko, E. S. Larin, V. V. Kirilenko and V. I. Pakhomov, *Sov. Phys. Solid State*, **30** (1988) 704.

[49] S. N. Kallaev, V. V. Gladkii, V. A. Kirikov, V. I. Pakhomov, I. N. Ivanova-Korfini and A. V. Goryunov, *Sov. Phys. Solid State*, **31** (1989) 1267.

[50] S. N. Kallayev, V. V. Gladkii, V. A. Kirikov and I. K. Kamilov, *Ferroelectrics*, **106** (1990) 299.

[51] V. V. Petrov, V. G. Pitsyuga, V. A. Gordeev, A. V. Bogdanova, M. A. Bagina and A. Yu. Khalakhan, *Sov. Phys. Solid State*, **25** (1983) 1995.

[52] A. A. Boguslavskii, R. Sh. Lotfullin, M. V. Simonov, V. V. Kirilenko, V. I. Pakhomov and A. Ya. Mikhailova, *Sov. Phys. Solid State*, **27** (1985) 321.

[53] A. V. Kityk, V. P. Soprunyuk, O. G. Vlokh, I. D. Olekseyuk and S. A. Piroga, *Sov. Phys. Solid State*, **34** (1992) 1091.

[54] A. V. Kityk, A. V. Zadorozhna, Ya. I. Shchur, I. Yu. Martynyuk-Lototska and O. G. Vlokh, *Phys. Stat. Sol. B*, **210** (1998) 35.

[55] A. V. Kityk Ya. I. Shchur, A. V. Zadorozhna, I. B. Trach, I. S. Girnyk, I. Yu. Martynyuk-Lototska and O. G. Vlokh, *Phys. Rev.* **B 58** (1998) 2505.

[56] A. V. Kityk, Ya. I. Shchur, A. V. Zadorozhna, I. B. Trach, I. S. Girnyk, I. Yu.

Martynyuk-Lototska and O. G. Vlokh, *Phys. Stat. Sol. B*, **211** (1999) 631.

[57] A. P. Levanyuk: *Incommensurate Phases in Dielectrics 1. Fundamentals*, ed. R. Blinc and A. P. Levanyuk, North Holland, Amsterdam, 1986, Chap. 1.

[58] M. Quilichini, J. P. Mathien, M. Le Postollec and N. Toupry, *J. Phys.*, **43** (1982) 321.

[59] V. I. Paknomov, N. M. Fedrova, I. M. Ivanova-Korfini, *Kood. Khim.*, **4** (1978) 1765.

[60] C. H. Townes and B. P. Dailey, *J. Chem. Phys.*, **23** (1955) 118.

[61] E. V. Shemetov, K. S. Aleksandrov, I. P. Aleksandrova and S. V. Primak, *Phys. Stat. Sol. A*, **104** (1987) K89.